Published in final edited form as:
J Cereb Blood Flow Metab. 2007 November ; 27(11): 1766–1791.

SUPPLY AND DEMAND IN CEREBRAL ENERGY METABOLISM: THE ROLE OF NUTRIENT TRANSPORTERS

Ian A. Simpson, Ph.D.[1], **Anthony Carruthers, Ph.D.**[2], and **Susan J. Vannucci, Ph.D.**[3]

1 *Neural and Behavioral Sciences College of Medicine, Penn State University, Hershey, PA 17033*

2 *Biochemistry and Molecular Pharmacology, University of Massachusetts Medical School, Worcester, MA, 01605*

3 *Department of Pediatrics, Columbia University, Morgan Stanley Childrens' Hospital of New York, New York, NY, 10032*

Abstract

Glucose is the obligate energetic fuel for the mammalian brain and most studies of cerebral energy metabolism assume that the vast majority of cerebral glucose utilization fuels neuronal activity via oxidative metabolism, both in the basal and activated state. Glucose transporter proteins (GLUTs) deliver glucose from the circulation to the brain: GLUT1 in the microvascular endothelial cells of the blood brain barrier (BBB) and glia; GLUT3 in neurons. Lactate, the glycolytic product of glucose metabolism, is transported into and out of neural cells by the monocarboxylate transporters: MCT1 in the BBB and astrocytes and MCT2 in neurons. The proposal of the astrocyte-neuron lactate shuttle hypothesis (Pellerin and Magistretti, 1994) suggested that astrocytes play the primary role in cerebral glucose utilization and generate lactate for neuronal energetics, especially during activation. Since the identification of the GLUTs and MCTs in brain, much has been learned about their transport properties, i.e. capacity and affinity for substrate, which must be considered in any model of cerebral glucose uptake and utilization. Using concentrations and kinetic parameters of GLUT1 and GLUT3 in BBB endothelial cells, astrocytes and neurons, along with the corresponding kinetic properties of the monocarboxylate transporters, we have successfully modeled brain glucose and lactate levels as well as lactate transients in response to neuronal stimulation. Simulations based on these parameters suggest that glucose readily diffuses through the basal lamina and interstitium to neurons, which are primarily responsible for glucose uptake, metabolism, and the generation of the lactate transients observed upon neuronal activation.

Keywords

glucose & lactate; glucose transporter proteins; mathematical modeling; monocarboxylate transporters; neurons & astrocytes; substrate delivery & metabolism

Introduction

The central dogma of cerebral energy metabolism is that glucose is the obligate energetic fuel of the mammalian brain and the only substrate able to completely sustain neural activity (Siesjo 1978). Furthermore, it has traditionally been assumed that the vast majority of cerebral glucose utilization fuels neuronal activity via oxidative metabolism, both in the basal and activated state (Sokoloff et al. 1977). Rates of cerebral blood flow (CBF) directly relate to measurements of cerebral oxygen consumption ($CMRO_2$), generating the concept of the "flow-metabolism

Address Correspondence to: Ian A. Simpson Ph.D., Professor, Neural and Behavioral Sciences MC H109, College of Medicine, Penn State University, C3801, 500 University Drive, Hershey, PA 17033, phone: (717) 531 4156, fax: (717) 531 5184, E-mail: ixs10@psu.edu.

couple" (Sokoloff 1976; Sokoloff et al. 1977). The introduction of neuroimaging techniques to study cerebral metabolism revealed an "uncoupling" between cerebral oxygen consumption, blood flow and glucose utilization during brain activation (Fox and Raichle 1986; Fox et al. 1988), with the suggestion of regional stimulation of oxidative glycolysis during neuronal activation. The temporal relationship between the release of lactate and the onset of neuronal activation, the source of the lactate i.e. neuronal or glial, and its subsequent diffusion and disposal, are all matter of considerable debate. Initial studies by Pritchard et al., (Prichard et al. 1991) assumed astrocytic and neuronal generation of lactate. A more recent proposal by Gjedde and colleagues (Gjedde and Marrett 2001; Gjedde et al. 2002) suggest that afferent neurons and astrocytes, rather than efferent neurons, are the source of lactate, whereas Fillenz (Fillenz 2005) suggests that lactate is released from astrocytes in response to the uptake of synaptically released glutamate. A very recent *in vitro* study investigated the relative significance of glucose and lactate as fuels to maintain neurotransmitter homeostasis during synaptic activity (Bak et al. 2006). They concluded that whereas lactate is capable of maintaining basal neuronal metabolism, glucose is the necessary substrate during synaptic activity. Structural considerations such as the relative dearth of mitochondria in both dendritic spines and the peripheral processes of astrocytes serve to further confuse the picture (Dienel and Cruz 2003; Sorra and Harris 2000). Studies by Dienel, Cruz and colleagues (Cruz et al. 1999; Dienel and Cruz 2003) have shown that lactate, wherever generated, is rapidly dispersed throughout the brain and into the bloodstream. Conversely the studies of Korf and others have shown the interaction of circulating lactate with neural lactate pools (Gjedde and Marrett 2001; Gjedde et al. 2002; Leegsma-Vogt et al. 2004; Leegsma-Vogt et al. 2003); Korf 2006; Fillenz 2005; Jones et al. 2000). The dogma has been further challenged by the astrocyte-neuron lactate shuttle (ANLS) hypothesis proposed by Magistretti, Pellerin, and colleagues, who postulated that astrocytes play the primary role in cerebral glucose utilization by metabolizing the glucose to lactate, which is subsequently transported to the neuron to fuel neuronal energetics (Pellerin and Magistretti 1994). During the decade since the ANLS was first proposed, there has been continual debate over whether neuronal activity is fueled primarily by glucose or lactate. There have been a plethora of reviews written specifically to either support or refute the ANLS hypothesis, without any apparent consensus (Aubert et al. 2005; Chih and Roberts 2003; Hertz 2004; Kimelberg 2004; Leybaert 2005; Magistretti and Pellerin 1999; Magistretti et al. 1999; Pellerin and Magistretti 1994; Pellerin and Magistretti 2003; Tsacopoulos and Magistretti 1996). Although some of these recent reviews mention the glucose transporter proteins (GLUTs) and the monocarboxylate transporter proteins (MCTs), little or no consideration has been given to the transport properties (capacity and affinity for substrates) of these transport systems and their relative contributions to substrate transport across the blood-brain barrier (BBB) and into the neural cells within the brain. The objective of this review is to address the role that transport may play in modulating cerebral metabolism, and the limitations that must be imposed on previously proposed models by the known concentrations and kinetic properties of the GLUT and MCT transporters in the brain. To this end we now propose a model that incorporates, where known, the kinetic properties and concentrations of the respective transporter proteins, as well as the role the basal lamina plays in the diffusion/delivery of glucose and lactate.

The transport of glucose and other hexoses into most mammalian cells is mediated by the SLC2 family of 13 transport proteins, GLUTs 1–12 and HMIT, the myo-inositol transporter (see (Joost and Thorens 2001; Uldry and Thorens 2004; Wood and Trayhurn 2003) for review). With the exception of GLUT1, which is ubiquitously expressed, the other family members have fairly distinct tissue- and cell-specific patterns of expression. Given the cellular heterogeneity of the brain, it is not surprising that most, if not all family members have been reported to be present in mammalian brain *in vivo* or *in vitro* preparations, as depicted in Figure 1. Much of the data supporting the indicated cellular distribution has been reviewed previously by us and others (Duelli and Kuschinsky 2001; Dwyer et al. 2002; Maher et al. 1994; Vannucci

et al. 1997), and will not be further discussed here. However, it is important to note that many of the transporters indicated in Figure 1 are either unable to transport glucose (GLUTs 5, 6, 11, & HMIT have very low affinity for glucose), or have very limited localization and concentrations (GLUT 2 & 4), while for others their location, ability and/or capacity to transport glucose has yet to be assessed (GLUTs 8 &10). Thus, with all of the above exclusions, the predominant transporters in mammalian brain involved in cerebral glucose utilization are GLUTs 1 and 3, which are expressed throughout the brain and whose localization and kinetic characteristics are well established. The cellular localizations of the glucose transporter proteins are shown together in Figure 1 with the relevant monocarboxylate transporters (MCTs), which are responsible for the transport of lactate, pyruvate, acetoacetate and β-hydroxybutyrate, and will be the focus of the remaining discussion.

Cerebral Glucose Utilization: GLUT1 and GLUT3

GLUT1 was the first glucose transporter to be cloned and whose kinetic characteristics have been most extensively studied (Mueckler et al. 1985). Two different molecular weight forms (45 and 55 kDa) of GLUT1 have been detected in mammalian brain. The difference in their relative molecular weight is accounted for by a differing extent of glycosylation (Birnbaum et al. 1986). However, these species do not appear to differ in their protein structure or kinetic characteristics (Birnbaum et al. 1986). The higher molecular weight 55 kDa form, which is comparable to that found in circulating erythrocytes of higher mammalian species, is found exclusively in the microvascular endothelial cells that make up the BBB where it is present in both the luminal and abluminal membranes, and in a substantial intracellular pool (see Figure 2) (Dick et al. 1984; Farrell and Pardridge 1991; Harik et al. 1990; Maher et al. 1992; Sivitz et al. 1989). Early studies in rat BBB endothelial cells reported an asymmetric distribution among these compartments: 11% luminal membranes, 44% abluminal membranes, and the remaining 45% residing in the intracellular pool (Cornford et al. 1993; Farrell and Pardridge 1991). Our own fractionation and kinetic studies, and more recent EM studies (Figure 2), support a more balanced distribution between the luminal and abluminal membranes, in agreement with Gerhart and colleagues (Gerhart et al. 1989; Simpson et al. 2001). Clearly, the ratio of luminal to abluminal GLUT1 transporters can have a direct effect on rates of glucose uptake into the brain, with increased luminal transporters supporting increased uptake (Simpson et al. 1999). A potential role of the intracellular pool in acute modulation of glucose transport across the BBB could be realized if these transporters were recruited to the luminal membrane in response to increased neural demand. Previous studies from our laboratory demonstrate that the increased cerebral glucose uptake observed in the chronically hypoglycemic rat is associated with both an increase in total endothelial GLUT1/mg microvessel protein, and specifically increased levels of luminal GLUT1 (Simpson et al. 1999). It will be important to devise other more acute *in vivo* paradigms to demonstrate whether translocation of transporters to the luminal membrane plays a role in acutely modulating glucose transport into the brain.

Although it was originally maintained that the only GLUT1 in the brain was in the BBB, Western blot analysis of vascular-free brain membranes yields a GLUT1 band at 45 kDa (Maher et al. 1992; Maher et al. 1994; Sivitz et al. 1989). The 45 kDa form of GLUT1 is found in all glial cells, as well as the basolateral and apical membranes of the choroid plexus, and ependyma. Another relevant aspect of the EM depicted in Figure 2 is the relative paucity of GLUT1 glucose transporters in the astrocytic endfeet adjacent to the endothelial cell. Under normal conditions there is very limited *in vivo* expression of 45kDa GLUT1 in neurons, although expression is increased in response to environmental stressors or when neurons are placed in culture (Gerhart et al. 1994; Lee and Bondy 1993; Maher et al. 1991;Wheeler et al. 1982).

GLUT3, originally cloned from a human fetal skeletal muscle cell line (Nagamatsu et al. 1992), was subsequently cloned from a variety of mammalian brain cDNA libraries, and in brain has been localized almost exclusively to neurons (Gerhart et al. 1992; Maher et al. 1992; McCall et al. 1994; Nagamatsu et al. 1993). Interestingly, peripheral sites of GLUT3 expression include sperm, platelets, placenta, and certain human gliomas; all cell types that exhibit high rates of glucose metabolism (see (Joost and Thorens 2001; Uldry and Thorens 2004; Wood and Trayhurn 2003). During cerebral maturation the increase in GLUT3 expression precedes the expression of the glial 45 kDa GLUT1 and is coincident with neuronal maturation, synaptogenesis, functional activity, and increased rates of cerebral glucose utilization (Vannucci 1994; Vannucci et al. 1993).

Kinetics of Glucose Transport

With the exception of the myo-inositol transporter which is proton driven, all of the GLUTs (1–12) are facilitative transporters. These transporters mediate energy-independent transport, which leads to glucose equilibration, but not glucose accumulation, by cells. However, these transporters catalyze bi-directional fluxes and the presence of intracellular and/or extracellular glucose alters the kinetics of transport both in and out of the cell. This bi-directional transport must be actively considered when modeling the flow of glucose from blood to the individual cells of the brain (See below and (Blomqvist et al. 1991; Carruthers 1990; Choi et al. 2001; Cloherty et al. 1996; de Graaf et al. 2001; Gjedde 1980; Gruetter et al. 1998; Hebert and Carruthers 1991; Qutub and Hunt 2005).

The capacity for glucose transport depends on the concentration of the transporter proteins as well as their intrinsic catalytic turnover activity or number of transport cycles catalyzed per transporter per sec (k_{cat}) within the respective cellular compartments. It is relatively easy to determine the total concentration of glucose transporters in brain microvessels, as these vessels are readily isolated from whole brain. Absolute concentrations of glucose transporter protein are determined by measuring the equilibrium binding of cytochalasin B. Cytochalasin B (CB) is a competitive inhibitor of GLUT1- and GLUT3-mediated glucose transport that binds to the intracellular glucose binding site of the transporters. Since CB is known to bind to other cellular proteins including actin, specificity of transporter concentration is achieved by measuring only that component of binding which is glucose-inhibited. Specificity is further enhanced by performing the assay in the presence of cytochalasin E which blocks binding to other cellular proteins but does not affect CB binding to the glucose transporters (Weber et al. 1988). Values for concentrations of GLUT1 in human and rat microvessels range from 40–125 pmol/mg protein (Kalaria et al. 1988; Vannucci et al. 1997). These values reflect binding to intact microvessels and include basement membrane and pericyte contamination. We have also measured binding to isolated bovine luminal and abluminal microvascular endothelial cell membranes and observe concentrations of 620 and 280 pmol/mg membrane protein, respectively (Simpson et al. 2001). Since CB binds to all glucose transporter isoforms, binding assays of whole brain fractions yield total glucose transporter values, i.e. both 55 and 45 kDa GLUT1, GLUT3, and even GLUT4, albeit in much lower concentrations (Kalaria et al. 1988; Maher and Simpson 1994; Maher et al. 1994; Simpson and Davies 1994). Such studies have revealed total transporter concentrations of 7 and 18 pmol/mg protein for human and rat brain, respectively. To further delineate GLUT1 and GLUT3 concentrations in whole brain samples, we employed a bis-mannose photolabel which, upon photoactivation, covalently modifies the transporter proteins with a radioactive tag 2-N-4[^{3}H] (1-azi-2,2,2 trifluroethyl) benzoyl-1,3-bis-(mannose-4yloxyl)-2-propylamine ([^{3}H] ATB-BMPA) (Maher and Simpson 1994). The different transporter isoforms were then isolated by immunoprecipitation and the quantity of radioisotope determined. Using this approach we concluded that the levels of (55 + 45) GLUT1 = GLUT3; 55 kDa GLUT1, 2.3–2.5 pmol/mg protein, 45 kDa GLUT1 6.9–7.7

pmol/mg protein, and GLUT3 8–11 pmol/mg protein (Maher and Simpson 1994; Vannucci et al. 1997).

The catalytic properties of GLUT1 have been studied most extensively in human red blood cells where cellular homogeneity and uniform cell size permit a level of accuracy in transport determinations that is not always possible with other cells. Human red cells are replete with the glucose transport protein GLUT1, containing approximately 2,000 copies per μm^2 (Gorga and Lienhard 1982). At sub-physiologic temperatures (0 – 24°C), GLUT1-mediated glucose transport is rapid and asymmetric (Lowe and Walmsley 1986). Asymmetry describes the relationship between K_m and V_{max} parameters for net glucose uptake and exit (Miller 1968; Widdas 1980). At 24 °C, V_{max} and K_m for D-glucose exit into glucose-free medium are approximately 4 -fold greater than the equivalent parameters for D-glucose uptake into glucose (Glc)-depleted cells (Baker and Naftalin 1979; Carruthers 1990; Karlish et al. 1972). This does not contravene the passive nature of GLUT1-mediated glucose transport. At very low [Glc], i.e. significantly less than the $K_{m,}$ the rate of glucose transport, v, is given by:

$$v = \frac{V_{max}[Glc]}{K_m + [Glc]} \approx \frac{V_{max}[Glc]}{K_m}$$

where [*Glc*] represents either intra- or extracellular glucose levels. Provided that the ratio V_{max}/K_m for exit = V_{max}/K_m for entry, the rate of glucose exit and entry will be identical at identical, subsaturating intra- and extracellular [Glc]. Glucose transport in cytosol-depleted human red cell ghosts is symmetric, i.e. V_{max} and K_m for D-glucose entry increase to match the equivalent parameters for exit (Carruthers 1986; Carruthers and Melchior 1983; Helgerson et al. 1989). In human erythrocytes, the GLUT1 activity is modulated by ATP which interacts allosterically to transform the intrinsically symmetric carrier into an asymmetric carrier (Carruthers and Helgerson 1989; Levine et al. 1998). Transport measurements in red cell ghosts show that the rate of net cellular export of 10 mM glucose into saline containing 3 mM glucose is inhibited 50% by intracellular ATP (i.e. when transport is asymmetric). Thus red cells, and presumably other GLUT1-expressing cells such as BBB endothelial cells, serve as less efficient glucose carriers when metabolically replete but efficiently transfer intracellular glucose to surrounding tissues when demand for glycolytic ATP is increased (Carruthers, 1986, Cloherty et al., 1996, Heard et al., 2000). GLUT1 transport asymmetry declines from 12-fold at 4 °C to 4-fold at 24 °C to 1.3-fold at 37°C (Lowe and Walmsley 1986).

GLUT3-mediated glucose transport is less extensively characterized than GLUT1-dependent transport. When expressed in *Xenopus* oocytes, GLUT3-mediated glucose transport demonstrates high affinity glucose transport relative to GLUT1 and GLUT2 (Colville et al. 1993; Rumsey et al. 1997). GLUT3-mediated transport in primary cultures of rat cerebellar granule cell neurons is characterized by high affinity, high capacity zero-trans glucose uptake at 24 °C (Maher et al. 1996). k_{cat} for GLUT3-mediated glucose transport ($V_{max}/[GLUT3]_{cell\ surface}$ = 880 per sec) is significantly greater than GLUT1 k_{cat} at 24 °C (151 per sec; (Lowe and Walmsley 1986)). If the observed 7.4-fold increase in GLUT1 k_{cat} for net glucose import between 24° and 37°C (Lowe and Walmsley 1986) is also observed with GLUT3, then k_{cat} for GLUT1 and GLUT3 at 37°C are 1,117 and 6,500 per sec, respectively (see Table 1). Interestingly, recent tissue culture studies of Barros and colleagues utilized the glucose analogs 2NBDG and 6NBDG, which are transported very slowly, to demonstrate that glutamate can reciprocally inhibit glucose uptake in neurons while promoting transport in astrocytes; the mechanism(s) by which these modulations are achieved i.e. alterations in k_{cat} or K_m and confirmation that they occur *in vivo* remain to be established (Loaiza et al. 2003; Porras et al. 2004). Although the fluorescent sugars are generally considered to be very poor substrates for GLUT1 (Cloherty et al. 1995), the authors demonstrate that NBDG transport is inhibited by the glucose transport inhibitor cytochalasin B. However, cytochalasin B also

inhibits the nucleoside transporter ENT1 (Leitch and Carruthers, unpublished) and ENT1 is known to modulate glutamatergic neurotransmission in the rat spinal dorsal horn (Ackley et al. 2003) raising the possibility that NBDG transport is not mediated solely by the GLUTs.

Monocarboxylate Transporters

The monocarboxylate transporters (MCTs) comprise the gene family SLC16, which has 14 members (Halestrap and Meredith 2004). However, of these 14 family members, only MCT 1–4 have been definitively shown to transport metabolically relevant monocarboxylic acids such as lactate, pyruvate, and the ketone bodies acetoacetate and β-hydroxybutyrate (Halestrap and Meredith 2004; Hertz and Dienel 2005; Pierre and Pellerin 2005). Moreover, as illustrated in Figure 1, all 4 are found in brain although MCT3 expression is limited to choroid plexus, and the pigment epithelial cells of the retina where it is abundant (Philp et al. 2001). The localization and kinetic characteristics of the MCTs in brain has been the subject of several recent reviews and we therefore will present only a brief synopsis here (Halestrap and Meredith 2004; Hertz and Dienel 2005; Pierre and Pellerin 2005).

MCT 1

The expression of MCT1 mRNA and protein are strongly developmentally regulated in the rodent brain. Early in postnatal development MCT 1 mRNA is widely expressed in all cell types, although the protein expression, particularly in neurons, appears more limited (Gerhart et al. 1997; Hanu et al. 2000; Leino et al. 1999; Pierre and Pellerin 2005; Pierre et al. 2000; Vannucci and Simpson 2003). This robust expression early in development coincides with the period of suckling and active ketogenesis in the rodent, and likely facilitates transport and utilization of ketone bodies (Hawkins and Biebuyck 1979; Nehlig and Pereira de Vasconcelos 1993; Vannucci and Simpson 2003). The relation between MCT1 expression, circulating ketone body concentrations, and cerebral utilization is most closely seen in the cerebral microvessels in which MCT1 expression reaches a peak at postnatal days 14–17, before falling to relatively low, adult levels by postnatal day 27; while the levels of MCT1 mRNA increase with development in astrocytes and decline in neurons, the MCT1 protein concentration in the parenchyma remains remarkably constant as the brain grows and develops (Vannucci and Simpson 2003).

MCT 2

The extent of MCT2 expression is species-specific because, while widely expressed in rodents, expression in human tissue is very restricted (Halestrap and Meredith 2004). In brain, initial *in situ* hybridization studies suggested that MCT2 was expressed almost exclusively in neurons (Gerhart et al. 1998; Koehler-Stec et al. 1998; Pellerin et al. 1998) and was detected in cultured neurons by immunohistochemistry as early as 1997 (Broer et al. 1997). However, it was not until 2002 that MCT2 protein expression was definitively localized to neurons in intact brain. These and subsequent studies have shown MCT2 to be extensively expressed in dendrites and associated with post synaptic densities (Bergersen et al. 2005; Pierre et al. 2002; Pierre and Pellerin 2005). Unlike MCT1, MCT2 mRNA and protein expression show little developmental response to changes in ketone body utilization (Vannucci and Simpson 2003). Rather, the developmental expression of MCT2 is similar to that of GLUT3 in that it increases in concert with cerebral maturation, synaptogenesis, and increases in glucose utilization.

MCT4

MCT4 has been extensively characterized in highly glycolytic muscle where it is responsible for lactate export. It is also expressed in chondrocytes, white blood cells, and in placenta where it exports lactate from the fetal circulation (Halestrap and Meredith 2004). In rodent brain

MCT4 is widely distributed yet appears to be localized exclusively to astrocytes (Bergersen et al. 2002; Rafiki et al. 2003).

Kinetics of MCT Transporters

The most definitive data on the kinetics of MCT1 were obtained from studies on human erythrocytes conducted long before the gene was cloned (see (Poole and Halestrap 1993) for review). These studies revealed that the transport of lactate proceeds by an ordered mechanism in which one proton binds to the transporter followed by one molecule of lactate, the protein undergoes a conformational change, and the lactate and then the proton are released on the other side of the membrane (Deuticke 1982; Dubinsky and Racker 1978; Leeks and Halestrap 1978). The K_s for the proton is 0.2 μM, which is equivalent to a pH of 6.7; the K_m for L-lactate when measured by zero trans uptake ranges from 4–13 mM (depending on pH); the K_m for efflux is 10.5 mM (De Bruijne et al. 1983; Deuticke 1982; Deuticke 1989). As with the GLUT1 glucose transporter, influx or efflux is accelerated by the presence of substrate on the opposite side of the membrane, i.e. 'trans acceleration' (Deuticke 1982). Subsequent studies in which MCT 1 was expressed in *Xenopus* oocytes confirmed K_m for pyruvate (0.7mM), L-lactate (3–5 mM), acetoacetate (4–6 mM), and β-hydroxybutyrate (10–12 mM; (Broer et al. 1998; Manning Fox et al. 2000)) (see Table 1).

Expression of MCT2 in *Xenopus* oocytes revealed it to be a proton-driven monocarboxylate transporter with a much greater affinity for lactate and pyruvate than MCT1, 3 & 4, with K_m of 0.7 and 0.1 mM, respectively (Broer et al. 1999; Dimmer et al. 2000; Lin et al. 1998). Kinetic analysis of MCT4 differs from that of MCT1 and MCT2 in that MCT4 has a higher affinity for lactate than pyruvate, although affinity for both substrates is significantly lower than that of MCT1–3, with a K_m for lactate and pyruvate of 28 and 150 mM, respectively, when rat MCT4 is expressed in oocytes (Manning Fox et al. 2000).

Several studies have been conducted to measure monocarboxylate transport in cultured neurons and astrocytes; however in all studies the simultaneous expression of more than one MCT isoform precludes a precise determination of activity of a given isoform. It is not surprising that MCT 1 is co-expressed with MCT2 in neuronal cultures, as most are prepared from embryonic or early postnatal brains where MCT1 is much more widely expressed. In some studies with neurons and synaptosomes, a low K_m for L-lactate (0.66–0.68 mM) has been observed in both, with corresponding V_{max} values of 3.4 and 4.2 nmoles/min/mg of protein, respectively (McKenna et al. 1998; Nedergaard and Goldman 1993). However, in both studies a second transport activity with a lower affinity and higher V_{max} activity was also observed which would appear more consistent with MCT1 expression. In other studies, no high affinity uptake was observed (Dringen et al. 1995). In the case of astrocytes, the wide range of K_m (7 to > 15 mM) and V_{max} (174–250 nmol/min/mg) values that have been observed can probably be attributed to the relative extents to which MCT1 and 4 are expressed in the particular culture (Broer et al. 1997; Manning Fox et al. 2000; Tildon et al. 1993).

Effects of pH on kinetics of MCT transporters

MCT1-catalyzed electroneutral proton-lactate co-transport is insensitive to membrane potential (Broer et al. 1998) but is sensitive to pH. At 4 mM intracellular and 1 mM extracellular lactate, net lactate export (computed using the general co-transport equation suggested by Stein (Stein 1986a) increases 1.4-fold ($pH_i = pH_o$) or 1.9-fold ($pH_o = 7.2$) when intracellular pH falls from 7.2 to 6.8. As intracellular lactate increases above $K_{m(app)}$ (4 mM), the effect of pH on net exit diminishes greatly.

MCT2-catalyzed electroneutral proton-lactate co-transport is also insensitive to membrane potential and is much less sensitive to pH at physiologic [lactate] (Broer et al. 1998). Thus at

1 mM [lactate] or greater (i.e. when [lactate] > $K_{m(app)}$), net lactate uptake is unchanged by extracellular pH in the range 5.5 to 7.5. These considerations indicate that while lactate-proton co-transport is influenced by intra- and extracellular pH, the overall impact of altered pH at physiologic [lactate] and pH is very small. Given the uncertainties associated with modeling pH changes and the observation that lactate transport is not greatly affected by pH, we made the simplifying assumption that intra- and extracellular pH are equal and constant.

Model for glucose and lactate flows in the mammalian brain

Having established the concentrations and kinetic parameters of the individual glucose and monocarboxylate transporters (Table 1), the objective of this review was to develop a new model of nutrient transport in the mammalian brain that incorporates these parameters. Figure 3A is an electronmicrogaph which depicts a typical cross-section through a microvascular endothelial cell and the adjacent parenchyma, indicating the proximity of the astrocytic endfeet and the neurons to the endothelial cell. Figure 3B is another electron micrograph, which depicts the potential diffusible spaces or compartments that need to be included in the kinetic model. The critical experimental component of Figure 3B is the inclusion of horseradish peroxidase, which was infused into the lateral ventricle, and clearly delineates the diffusible spaces (Brightman and Reese 1969). The importance of this early study is the demonstration of the accessibility of the basement membrane, or more completely the basal lamina, to relatively large molecules. Thus, it is clear that smaller molecules such as lactate and glucose will also enter and readily diffuse within this space, and rapidly distribute along the entire basal lamina providing an effective conduit to both neurons and astrocytes. The basal lamina is an integral component to the model we propose to describe the passage of glucose and lactate into neurons and glia (Figure 3C).

As depicted in Figure 3C, glucose enters the mammalian brain and equilibrates with the basal lamina via rapid facilitated transport across the endothelial cell layer of the BBB. We model two potential outcomes from this point. Pathway 1, which does not include diffusion through the basement membrane, shows glucose entering the astrocyte where it can be converted to lactate as proposed by the astrocyte-neuron lactate shuttle hypothesis (ANLS) (Magistretti and Pellerin 1997), and subsequently transported into the interstitium. Another possibility within pathway 1 is that glucose enters the astrocyte, traverses the cell and is transported out, unchanged, into the interstitium. Lactate or glucose can then be transported into adjacent neurons. An alternative hypothesis is posed by pathway 2 of Figure 3C, which proposes that basal lamina glucose diffuses freely into the astrocytic endfoot and the interstitium whence it is transported directly into astrocytes and neurons. The purpose of our model building is to examine these hypotheses by application of transport theory.

Mass transport of glucose and lactate

Two mass transport processes are considered, free diffusion and carrier-mediated facilitative transport. The free diffusion of glucose is analogous to Stokesian diffusion of small molecules in aqueous solution in which the diffusion coefficient, D, is given by:

$$D = \frac{kT}{6\pi\eta r} (cm^2 \, per \, sec)$$

where k is the Boltzman constant, T is temperature (°K), η is the viscosity of the solvent and r is the molecular radius of glucose. The tortuosity of the brain's extracellular space (λ) represents the hindrance imposed on diffusing molecules by the tissue in comparison with an obstacle-free medium (Hrabetova and Nicholson 2004). A value of 1 would indicate an absence of such hindrance. The apparent diffusion coefficient (D_{app}) for molecular-self-diffusion in the brain is thus given by:

$$D_{app} = \frac{D}{\lambda} cm^2.s^{-1}$$

where λ has been measured experimentally to be 1.6 (Hrabetova and Nicholson 2004). This value is significantly greater than the 1.25 that would have been predicted based on their model building and reflects so called 'dead-end spaces' which lead to a restriction of specific flow. The value of 1.6 refers to diffusion within cortex; greater values have been reported for hippocampus and cerebellum, and in pathological situations such as ischemia (Nicholson 2005; Tao et al. 2005; Tao et al. 2002; Tao and Nicholson 2004). However, even with the experimentally determined limitations, it is clear that small molecules such as glucose and lactate can rapidly diffuse throughout the interstitium, as illustrated in Figures 3 A & B. The rate constant (k_{app}) for molecular diffusion between two points (separated by ϕ cm) in space is given by:

$$k_{app} = \frac{D_{app}}{\phi^2} (per\ sec)$$

Thus for D-glucose ($D = 7 \times 10^{-6}$ $cm^2.s^{-1}$ at 37°C), $D_{app} = 4.4 \times 10^{-6}$ $cm^2.s^{-1}$ and k_{app} for diffusion across 25×10^{-4} cm (the average midpoint between adjacent brain capillaries) is 0.7 per sec ($t_{½}$ = 1 sec). An important question concerns small molecule diffusion between cells. As illustrated in Figure 3B the distribution of horseradish peroxidase clearly demonstrates that the marker equilibrates throughout the interstitial space, up to and including the basal lamina. This suggests that molecular diffusion of horseradish peroxidase (MW= 40,000) and, by inference, of D-glucose (MW = 180.16) between astrocytes is not limiting. Given that a first order process is more than 92% complete within 4 half-lives, the data above suggests that in the absence of glucose consumption, basal lamina and interstitial glucose attain 92% equilibration within 4 sec. The rapidity of this diffusion defines pathway 2.

Analyses of steady-state, carrier-mediated glucose transport typically address two specific transport conditions: zero-trans and equilibrium exchange transport (Lieb and Stein 1972). In zero-trans transport, glucose is absent at the opposite or trans-side of the membrane, while it is varied at the originating or cis-side of the membrane. Thus, for zero-trans entry, intracellular glucose is absent and extracellular glucose is varied to obtain V_{max} and $K_{m(app)}$ for zero-trans entry. In equilibrium exchange, intracellular [Glc] = extracellular [Glc] and radio-tracer glucose is added at zero-time to initiate the transport measurement. The rate constant for radio-tracer equilibration is measured as a function of unlabeled [Glc] to obtain V_{max} and $K_{m(app)}$ for equilibrium-exchange.

Mathematical descriptions of carrier-mediated passive transport reduce to a single equation comprising constants derived from these measurements of V_{max} and $K_{m(app)}$ (Carruthers 1991; Stein 1986a). These constants include an affinity term (K) and four resistance terms (R_{oo}, R_{ee}, R_{io} and R_{oi}), where R is defined as the inverse of V_{max}. Three of these resistance terms (R_{ee}, R_{io} and R_{oi}) are measured directly as $1/V_{max}$ for equilibrium-exchange, zero-trans exit, and zero-trans entry respectively. For example, if V_{max} for zero-trans D-glucose uptake in primary, neuronal cultures was measured as 32 pmol/10^6 cells/sec, R_{oi} for transport would be $1/V_{max}$, which is 3.2×10^8 sec/10^6 cells/mol. If V_{max} for zero-trans D-glucose uptake in primary astrocytic cultures was measured as 9 pmol/10^6 cells/sec, R_{oi} for transport would be $1/V_{max}$ which is 11×10^8 sec 10^6 cells/mol. Thus the resistance term R is inversely related to V_{max}; the greater the resistance parameter, the lower the cellular glucose transport capacity.

The transport equation is:

$$v^{oi}_{net} = \frac{Glc_o(K + Glc_i) - Glc_i(K + Glc_o)}{K^2 R_{oo} + KR_{oi}Glc_o + KR_{io}Glc_i + R_{ee}Glc_oGlc_i}$$

with the constraint $R_{oo} = R_{oi} + R_{io} - R_{ee}$

where Glc is glucose concentration, o and i refer to extra- and intracellular respectively, and where v^{oi}_{net} is the steady-state rate of net glucose transport in the direction of extracellular to intracellular. Because the resistance terms are related to V_{max} for transport, this transport equation describes both cellular affinity (K term) and capacity (R terms) for glucose transport. The equation for lactate transport includes a multiplicand $[H^+]$ term associated with each [lactate] term (see Appendix Table 2 and (Carruthers 1991; Stein 1986a)) but we assume that $[H^+]_i = [H^+]_o = 63$ nM (pH 7.2).

Table 1 presents transporter concentrations, k_{cat}, $V_{max,}$ and K_m parameters for glucose and lactate transport by endothelial cells, astrocytes, and neurons at 37°C. Appendix Table 3 summarizes R and K parameters for glucose and lactate transport by endothelial cells, astrocytes, and neurons at 37°C. In some instances, such as lactate transport and red cell and neuronal glucose transport, constants are computed directly from measurements of V_{max} for transport. In other instances, such as glucose transport in endothelial cells, astrocytes, and neurons, identification of the cell membrane glucose transporter species (e.g. GLUT1 or GLUT3) and concentration (based on CB binding measurements) are sufficient to compute R parameters because the properties of GLUT1 and GLUT3 have been described accurately in other systems. Although lactate transport is mediated by H^+/lactate symport (Halestrap and Meredith 2004;Halestrap and Price 1999), we cannot describe all transmembrane proton gradients with an acceptable degree of confidence. We thus model lactate transport as lactate/H^+ symport in the absence of a transmembrane H^+ gradient. MCT k_{cat} is not known because cell surface [MCT] has not been measured in cells where lactate transport has been quantified. MCTs are members of the Major Facilitator Superfamily (MFS) of transport proteins (Saier et al. 1999) and k_{cat} may approach that of GLUT1 (another MFS protein). We therefore assigned each MCT a k_{cat} value identical to that of GLUT1 (1166 per sec). In support of this assumption it should be noted that V_{max} for lactate transport in human red cells (2 mM/min; (Pattillo and Gladden 2005)) is approximately 100-fold lower than V_{max} for lactate transport in rabbit red cells which contain approximately 156,000 copies of MCT protein (Jennings and Adams-Lackey 1982). This suggests that MCT k_{cat} = 1,000 per sec, in good agreement with our designation of 1166 per sec.

Cellular Glucose Transporter Concentrations

Examination of Table 1 reveals that the capacity (V_{max}) of GLUT1 in the microvascular membranes of the BBB is dramatically higher than in either the astrocyte or neuron. These determinations of transport capacity come from measurements of CB binding to membranes isolated from neurons, astrocytes, and endothelial cells (Vannucci et al. 1997) and from transport measurements (Maher and Simpson 1994;Maher et al. 1991;Maher et al. 1994). As discussed above, high affinity CB binding to endothelial cells, astrocytes, and neurons is a good measure of the glucose transporter content of membranes from these cells because glucose uptake is quantitatively inhibited by CB in each of these systems. Thus, astrocytes contain 5.8 to 7.3 pmol CB binding sites/mg membrane protein (Keller et al. 1986;Vannucci et al. 1997); endothelial cells contain 400 pmol CB binding sites/mg membrane protein (Simpson et al. 2001); neurons contain 9.5 pmol CB binding sites/mg membrane protein (Maher et al. 1996). Based on the CB binding content and glucose transport capacity of rat cerebellar granule neurons, and the identity of their major glucose transport species as GLUT3, Maher et al conclude that GLUT3 k_{cat} is some 8-fold greater than GLUT1 k_{cat} (Maher et al. 1996). Whilst

the neuronal CB binding capacity is comparable to that of the astrocyte, the kinetic parameters of GLUT3 (K_m 2.8 mM; k_{cat} 6,512 per sec) result in an overall increase in glucose transport capacity relative to GLUT1-expressing astrocytes (K_m 8 mM; k_{cat} 1,166 per sec). Based on these numbers, the glucose transport capacity of membranes isolated from neurons is at least 9-fold greater than that of astrocytic membranes at 5 mM [Glc].

Geometries and metabolism

To examine this further, we next consider brain "geometry", cellular composition, and cellular metabolic profiles. Our model assumes a simple 2 × 2 × 17 μm section into the brain from the capillary lumen (Figure 3C). Dimensions are arbitrary but are based on the observations in rat cortex that: 1) neurons occupy 49%; 2) astrocytes occupy 25%; 3) interstitial space is 20% of the brain volume (Hrabetova and Nicholson 2004; Maher and Simpson 1994). Cell volumes, plasma membrane protein (GLUT1, GLUT3, etc) contents, and cell total protein content, are based on previously measured parameters obtained with neurons, astrocytes (Maher et al. 1996; Vannucci et al. 1997), and human red cells (Carruthers 1986). Our calculations assume: 1) cell protein content = 10% cell mass; 2) primary cultures of neurons are composed of cells of average volume = 2 pL; 3) RBC surface area = 144 μm^2; 4) RBC volume = 90 fL; 5) neuron GLUT3 content = 9.5 pmol/mg membrane protein; 6) neurons in primary culture contain 20 μg total protein per 10^6 cells (Maher et al. 1996). Table 1 summarizes our calculations of endothelial, neuronal, and astrocytic GLUT contents.

Metabolic activity is modeled assuming simple one-step Michaelis-Menten steady-state kinetics for glucose conversion to lactate and simple one-step Michaelis-Menten steady-state kinetics for lactate conversion to CO_2. For example, glucose conversion to lactate is described by:

$$^{V}Glc-L = \frac{V_{mh} \cdot G}{K_{mh} + G}$$

where V_{mh} is V_{max} for conversion of 1 glucose into 2 lactate molecules and K_{mh} is $K_{m(app)}$ for phosphorylation of glucose by hexokinase (≈ 40 μM glucose (Whitesell et al. 1995; Wilson 2003). Glycolysis and oxidative metabolism are known to be more complex than these simplifications allow; for a comprehensive analysis of astrocytic and neuronal glucose metabolism see (Aubert and Costalat, 2005). However, these expressions are not introduced to simulate the detailed regulation of metabolic flow. Rather they are used to permit a simple but saturable flow of glucose and lactate into glycolytic and oxidative pathways respectively. During neuronal stimulation, glycolysis in neurons and/or astrocytes is modeled to undergo a brief (45 sec) 3- to 4-fold increase. This is preceded by a shorter (25 second) 1.4-fold increase in neuronal and astrocytic lactate oxidation.

Several studies have reported relative rates of glucose and lactate transport and metabolism in neurons and astrocytes. In mice, rats, and humans the brain metabolizes glucose at an average rate 80, 74, and 100 μmol/100 g brain per min, respectively (Brown and Lorden 1989; Choi et al. 2001; Itoh et al. 2001). The ratio of glucose uptake: glucose metabolic capacity is 2.7 ± 0.1 (Choi et al. 2001). In our primary model, outlined in Figures 4, 5 & 6, with serum levels of glucose and lactate at 6 mM and 1 mm, respectively, the simulated sum of neuronal and astrocytic glucose utilization is 80 μmol/100 g brain per min. The model also assumes that the ratio of steady-state glucose uptake: glucose metabolism is 1:1, the K_m for simulated net glucose import is 10 mM, and that glucose utilization is saturated at [Glc] greater than 0.5 mM. Thus, at 6 mM [Glc], the ratio of glucose import : utilization capacity is 2.7:1, which is a result consistent with the reported value of 2.7 (Choi et al. 2001).

Flows between compartments

Figure 4 models the flow of glucose (left) and lactate (right) from serum to neurons. The transporter catalyzing each flow is indicated next to each arrow. Flows between compartments are described in Appendix Table 1 and are indexed by a number and are fully annotated in Appendix Table 2. Equation parameters are defined in Appendix Table 3.

Model simulations were performed by 4th order Runge Kutta numerical integration using the software package Berkeley Madonna (version 8.3.12; http://www.berkeleymadonna.com). Time-dependent increases in glycolysis and lactate oxidation were simulated by introducing square-wave pulses in V_{max} for glycolysis and lactate oxidation. The model is available as a text file of differential equations and is accessible via a link in the Appendix.

Simulations and Results

Using the proposed model we posed the following questions:

1. What are the predicted steady-state brain glucose and lactate levels and how do these compare with observed values?
2. What is the net effect of diffusion through the basal lamina on glucose uptake into the brain, i.e. net flux via pathway 1 vs pathway 2 as depicted in Figure 3C?
3. What is the effect of neuronal activity on lactate transients in the brain? What are the relative astrocytic and neuronal contributions to these lactate levels?
4. What properties of the model must be altered in order to simulate the predictions of the ANLS hypothesis?

Brain glucose levels represent a net balance between glucose uptake from the circulation (serum) and glucose metabolism to lactate, CO_2, and other metabolites, as well as glucose transport back to the circulation. Glucose movements between CSF and interstitium are not considered here. The baseline parameters of the model are summarized in Table 1 and Appendix Table 3. These parameters fall into three categories: A) transport capacities/ affinities; B) glucose utilization capacities; C) lactate utilization capacities. The core model utilizes previous estimates of cellular GLUT and MCT contents and transport measurements to establish transport capacities and affinities. The values in Table 1 and Appendix Table 3 support the following statements: 1) neurons transport glucose with 12-fold greater capacity (V_{max}) than do astrocytes; 2) lactate transport capacities of neurons and astrocytes are very similar; 3) neuronal and astrocytic glycolysis and glucose transport are related through a 'glycolytic coupling factor' or GCF, which is proportional to $V_h \cdot R_{oi}$ or V_{max} for glucose utilization/V_{max} for zero-trans glucose uptake. GCF prevents the ratio for total brain glucose import: glycolytic capacity from falling below 2.7:1 (Choi et al. 2001); this is important because experimental brain total glucose levels of 9 mM observed at 30 mM serum glucose (Choi et al. 2001;Gruetter et al. 1998) would not otherwise be possible; 4) lactate utilization is proportional to lactate production and lactate transport in neurons and astrocytes. This is established through an 'oxidation coupling factor' or OCF, which is proportional to $V_L \cdot R_{oi}$ or V_{max} for lactate utilization/V_{max} for zero-trans lactate uptake. OCF ensures that lactate cannot be consumed faster than it is produced and/or imported by the cell. The OCF which permits the most accurate simulation of experimental data by the model is 0.1. It should be emphasized that GCF and OCF are simulation constants that permit net balance of transport and metabolic flows.

Simulation 1 - brain steady-state glucose and lactate levels (Questions 1, 2)

The first challenge we presented to the model was simulation of basal brain steady-state glucose and lactate levels. Figure 5 summarizes our results. Our simulations varied the starting serum glucose levels from 1 to 30 mM, and were permitted to run until steady-state total glucose levels were achieved. These simulations (5A) predicted a very close correspondence between theory and data obtained in rats and humans (Choi et al. 2001;Gruetter et al. 1998), but only when path 2 (see Fig 3C) was permitted. Table 2 summarizes the predicted [Glc] of each brain compartment at 6 and 30 mM serum [Glc]. Under basal conditions and at 6 mM serum glucose, astrocytic lactate utilization is two-fold greater than astrocytic lactate production, leading to net lactate import from the interstitium (see Fig 5 B). Neuronal glucose and lactate utilization are 5- and 2.5-fold greater than astrocytic glucose and lactate utilization, respectively (see Fig 5 B). If basal lamina to interstitium diffusion is not permitted (only path 1 of Figure 3C is operational), simulated total brain [Glc] approaches 10% of experimental values (dotted line, Figure 5A); interstitial [lactate] is dramatically reduced as discussed below. When diffusion is eliminated, net glucose transport at steady-state from serum (6 mM glucose) to basal lamina is reduced by 13-fold, while basal lamina [glucose] approaches equilibrium with serum glucose as 5.7 mM. When diffusion is permitted, steady-state basal lamina glucose falls to 2.1 mM because paracellular glucose diffusion circumvents the potential resistance barrier posed by the low transport capacity of the astrocytic endfoot (see Figure 2). Glucose can diffuse from the basal lamina to the interstitium where it is transported into, and utilized by, both neurons and astrocytes. Without paracellular diffusion between basal lamina and interstitium, successful simulation of experimental steady-state and transient glucose and lactate levels is not possible. Transport through the astrocyte thus represents a significant barrier to overall glucose uptake by the brain. It is important to note that diffusion between the basal lamina and interstitium is 92% complete within 4 sec (see page 19). Thus, paracellular diffusion would short-circuit the astrocytic barrier to glucose uptake and facilitate rapid and extensive glucose equilibration between basal lamina, interstitium, and neuronal compartments.

Simulation 2 - lactate transients and neuronal activity (question 3)

Brain interstitial lactate levels are known to undergo a significant but transient increase following neuronal stimulation (Hu and Wilson 1997). We simulated the effects of neuronal stimulation by introducing a 25-sec burst of neuronal lactate oxidation (a 1.4-fold increase) followed by a 45 sec burst of neuronal and astrocytic glycolytic activity (a 4.3-fold increase) at a time (1000 sec) when brain glucose levels have reached steady-state with serum glucose (6 mM). The oxidative pulse briefly lowers neuronal and interstitial lactate levels while the glycolytic pulse transiently depletes neuronal [Glc] by 5-fold and increases interstitial [lactate] almost twofold, from 1.0 to 1.8 mM. Upon cessation of stimulation, neuronal [Glc] and interstitial [lactate] recover with a half-time of approximately 90 sec (Figure 6). This result is very similar to the experimentally reported behavior of interstitial lactate (Choi et al. 2001; Hu and Wilson 1997). In the absence of paracellular diffusion, steady-state interstitial lactate levels are significantly lower (0.05 mM) and the lactate transient produced by elevated glycolysis is eliminated (Figure 6). Upon cessation of enhanced glycolysis, the return to baseline is determined by the steady-state kinetics of lactate transport and lactate utilization. We address the sources of interstitial lactate in more detail below (Figure 8).

The following simulations were designed to specifically address question 4, i.e. what properties of the model must be altered to simulate the predictions of the ANLS?

Simulation 3 – Basal lamina to interstitium diffusion is operational and astrocytes and neurons transport glucose with equal efficiency

We next simulated a scenario in which astrocytic and neuronal glucose transport capacities are identical and where paracellular diffusion from the basal lamina to interstitium is permitted.

We further imposed a condition in which neuronal glycolysis was assumed to be unresponsive to increased electrical activity (stimulation). This scenario models a central tenet of the ANLS hypothesis, which holds that neuronal stimulation activates astrocytic glycolysis which generates lactate to fuel neuronal lactate oxidation. In order to recapitulate the results of Figures 5 and 6, astrocytic glucose transport capacity must be increased to levels 12-fold greater than those predicted to occur based on GLUT1 glucose transporter measurements. Several metabolic adjustments are also necessary. These are: 1) astrocytic glycolytic capacity is increased by 21%; 2) astrocytic and neuronal lactate oxidation capacity and neuronal glycolytic capacity are increased very slightly (4%). Figure 7 summarizes the results of these simulations and the changes in glucose and lactate flows in neurons and astrocytes. The results of Figure 5 and 6 are recapitulated by these adjustments to the model. Under basal conditions, the neuron remains a lactate exporter and the astrocyte a lactate importer. Astrocytic endfoot glucose import is increased by 6-fold at 6 mM blood glucose but glucose utilization by the astrocyte is only slightly (5%) increased. However, the adjusted model shows a major change in behavior during the neuronal stimulation-induced lactate transient.

Figure 8 illustrates these changes in lactate transients. The core model (based on measured GLUT contents and permitting increased neuronal glycolysis during neuronal stimulation; Figure 8A), shows that interstitial lactate is derived largely from neuronal export of lactate. Net flow of lactate from interstitium to basal lamina by diffusion is low but significant and astrocytes undergo net uptake of interstitial lactate. During the brief (25 sec) stimulation-induced oxidative burst, neuronal lactate levels fall rapidly causing a net decrease in lactate export to the interstitium with a resultant decrease in interstitial [lactate]. During the stimulation-induced glycolytic burst immediately following the oxidative response (neuronal and astrocytic glycolysis are quadrupled for 45 sec), neuronal, astrocytic, and consequently interstitial glucose are rapidly reduced by 75%. Neuronal lactate levels increase 2-fold resulting in net lactate export to the interstitium whence it is imported by the astrocyte. The major source of interstitial lactate during the transient is neuronal.

When the basic model is modified to increase astrocytic glucose transport capacity 12-fold and to render the neuron glycolytically unresponsive to stimulation (see parameters of Figure 7), the neuron still exports lactate and the astrocyte imports lactate under basal conditions (Fig 8B). During the brief (25 sec) stimulation-induced oxidative burst, astrocytic and neuronal lactate levels fall rapidly. This reduces neuronal lactate export to the interstitium causing a reduction in interstitial lactate. During the stimulation-induced glycolytic burst immediately following the oxidative response (astrocytic glycolysis is increased by 14.4-fold for 45 sec) astrocytic glucose is rapidly depleted. As a consequence, interstitial glucose is reduced by 60%; neuronal glucose falls in response to reduced glucose import in the face of continued glycolysis. Increased astrocytic lactate production leads to lactate export into the interstitium. Reduced neuronal glucose limits endogenous substrate for neuronal lactate production causing the neuron to import lactate from the interstitium. Thus the astrocyte supplies lactate to the neuron during stimulation because it indirectly exhausts the neuron's supply of glucose. This effectively recapitulates the ANLS model proposed by Pellerin, Magestretti and colleagues in that, upon neuronal stimulation, the astrocytes produce lactate which is taken up by the neurons. For this to be a viable model it requires paracellular diffusion and a substantial increase in astrocytic glucose transport capacity. Since CB binding studies support a limited concentration of total GLUT1 & GLUT3 glucose transporters in isolated glial/neuronal membranes, the increased transport capacity must be mediated by a transporter other than GLUT1 that does not bind cytochalasin B. However, our own transport studies in cultured astrocytes have indicated that the vast proportion of 2-deoxyglucose uptake is inhibited by cytochalasin B (data not shown), suggesting that expression of the requisite transporter is either lost upon culturing the astrocytes or non-extant.

Simulation 4 - No diffusion from the basal lamina to interstitium and the necessary compensations (pathway 1 of Figure 3C)

This simulation models the two central tenets of the ANLS hypothesis: 1) neuronal activation stimulates astrocytic glycolysis, which supplies lactate for neuronal oxidation; 2) glucose passes through the astrocyte to access the interstitium (paracellular diffusion is not permitted; only pathway 1 of Figure 3C is operational). The purpose of this simulation was to investigate which adjustments in astrocytic glucose transport are necessary for brain glucose and lactate levels to respond normally to alterations in serum [glucose] and to neuronal stimulation. We further imposed the condition where neuronal glycolysis is unresponsive to stimulation while the astrocyte responds with increased glycolysis.

We successfully mimicked the simulations of Figures 5 and 6 in the absence of diffusion by increasing astrocytic glucose transport by 100-fold. It was necessary to reduce neuronal and astrocytic glucose utilization by 5 and 80%, respectively and to increase neuronal and astrocytic lactate utilization by 7% and 5%, respectively, in order to prevent un-physiological accumulation of interstitial lactate (Figure 9). Under these conditions, the astrocytic endfoot imports glucose 67-fold faster than in Figure 5 and the astrocyte exports glucose into the interstitium for increased net uptake by the neuron. In essence, an astrocyte with high glucose transport and low glucose utilization capacities serves as a conduit for glucose delivery to the interstitium. These parameter changes permit faithful reproduction of the experiments depicted in Figures 5 and 6 and simulated with the primary model. The neuron remains the major (90%) source of lactate production and consumption both at rest and during stimulation. The neuron is the major source of interstitial lactate at rest whereas the astrocyte is the major source of interstitial lactate during stimulation. This simulation together with the data presented in figure 5, in which the effects of eliminating paracellular flux were also investigated, clearly suggest that transport of glucose exclusively through the astrocytic endfoot is not a viable option.

Comparison with other models

Several investigators have considered models for steady-state and transient lactate and glucose distributions in the brain. Fillenz critically evaluates the ANLS hypothesis and concludes that the thermodynamic cost of glutamate uptake by astrocytes (3% of brain ATP consumption) is insufficient to stimulate astrocytic glycolysis and lactate production from glucose (Fillenz 2005). The author proposes that the initial dip in interstitial lactate upon neuronal stimulation results from increased neuronal oxidative metabolism, coincident with a simultaneous increase in neuronal glycolysis, causing glucose levels to decline, consistent with our model (see Figure 6). However, the author further hypothesizes that neuronal stimulation causes astrocytes to release glutamate, which leads to intracellular astrocytic Ca^{2+} waves causing increased lactate production and release. This latter event is much slower than neuronal activation and correlates with the slow increase observed in astrocytic NADH levels.

Gjedde and Marrett argue that glycolysis in neurons, not astrocytes, delays oxidative metabolism in the stimulated visual cortex (Gjedde and Marrett 2001). In addition, and in agreement with our premise, the authors argue that astrocytic endfeet are not an integral part of the blood -brain barrier and thus do not restrict the use of glucose to astrocytes. They propose that astrocyte metabolism is not less oxidative than that of neurons (Gjedde and Marrett 2001), and conclude that neuronal stimulation increases both neuronal and astrocytic glycolysis and O_2 consumption.

Leegsma-Vogt et al., measured and simulated cerebral arteriovenous lactate kinetics after intravenous lactate infusion in the rat (Leegsma-Vogt et al. 2004). Their data supports a model in which serum lactate exchanges with a brain lactate compartment that represents approximately 24% of brain volume. Since astrocytic, neuronal, and extracellular

compartments are 25%, 50%, and 20% respectively of brain volume (Aubert and Costalat 2005), this exchangeable compartment could represent ECF, astrocytes or a sub-fraction of total neurons. Aubert and Costalat present a detailed and lucid analysis of glucose, lactate, and pyruvate metabolism in brain (Aubert and Costalat 2005). Their model assumes glucose exchange between 4 major compartments: capillary, extracellular space, astrocytes, and neurons. Their model differs from the present study by combining the basal lamina and interstitium as a single compartment but, as with the present model, diffusion of glucose between the extracellular space adjacent to capillaries and neurons is not limiting. In the current study the rates of astrocytic glucose transport are proposed to be 12-fold slower than neuronal glucose transport, compared to a 5-fold difference proposed by Aubert and Costalat (Aubert and Costalat 2005). Their model does not use standard carrier-mediated transport equations for glucose uniport or lactate/proton symport; the consequences of known differences in affinity of GLUT1 and GLUT3 for glucose or of MCT1 and MCT2 for lactate are not considered (Stein 1986b). The other major distinction between the two models is that in the present model, glucose transport across the endothelial cell appears to be considerably faster.

Aubert et al., investigate models for the very rapid lactate transients observed in rat hippocampus after electrical stimulation of the perforant pathway as described by Hu and Wilson (Aubert et al. 2005; Hu and Wilson 1997). These kinetics (see Figure 6) show a brief decrease in interstitial [lactate] followed by a 1.8-fold increase, which then returns to baseline levels over a period of 500 sec. The authors conclude that these 3 phases represent: 1) an initial increased brain lactate oxidation, as also observed by Kasischke et al., (Kasischke et al. 2004); 2) a sustained increase in lactate production which, upon termination of increased glycolysis; 3) is followed by lactate oxidation and uptake by cells. The authors successfully simulate the observed kinetics and, like us, conclude that local changes in cytoplasmic and interstitial pH have only a very small effect on net lactate distributions. They also conclude that the greater $K_{m\ (app)}$ for MCT1-catalyzed lactate transport in astrocytes favors export by astrocytes rather than high affinity MCT2-catalyzed export by neurons. We would disagree with this conclusion because high affinity, high capacity MCT2-catalyzed lactate export produces greater transport rates at physiologic [lactate]. Their conclusion may have arisen from the failure to use appropriate carrier-equations for symport (Stein 1986b).

In this study we have manipulated our proposed model to accommodate the predictions of ANLS, and to delineate the potential changes in transport capacities that are necessary to fit the published data of Greutter and colleagues and Hu and Wilson as illustrated in Figures 5 & 6 {Choi, 2001 #280; Gruetter, 1998 #583; Hu, 1997 #3814}. For the model to accommodate the ANLS hypothesis, where the astrocyte is the primary source of lactate production and the neuronal glycolytic burst response to stimulation is eliminated, the following compensatory adjustments to the model are necessary: 1) astrocytic glucose transport is increased 13-fold to quantitatively match neuronal glucose transport when paracellular glucose diffusion from basal lamina to interstitium is permitted; 2) astrocytic glycolysis and lactate oxidation, and neuronal lactate oxidation are increased (Figures 7 & 8B). Measured physiologic levels of astrocytic GLUT1 cannot meet these requirements, thus necessitating the hypothetical participation of additional glucose transporter proteins, such as GLUT6 and GLUT9, which have been identified but as yet have not been characterized (Augustin et al. 2004; Doege et al. 2000). It is important to note, however, that the additional transporters, if present, are inhibited by CB because astrocytic glucose uptake is completely inhibited by CB, and thus should have been detected in astrocyte CB and photolabel experiments. Our attempts to recapitulate the ANLS hypothesis by reducing neuronal glucose transport capacity to the level of the astrocyte were unsuccessful (data not shown). Constraining the passage of glucose solely through the astrocytic endfoot (pathway 1 of Figure 3C), as most commonly drawn diagrammatically when ALNS is illustrated, results in dramatic reductions in total brain glucose and lactate levels (Figure 5). For this pathway to become viable it is necessary to elevate astrocytic glucose

transport 100-fold over predicted values in order to mimic experimental observations (Figure 9). Under these conditions: 1) glucose must be transported into the astrocyte and then exported to the interstitium to enter neurons; 2) interstitial lactate derives from neurons under resting conditions, and from astrocytes during neuronal stimulation, assuming that neuronal glycolysis is not activated during neuronal stimulation. If neuronal and astrocytic glycolysis respond equally to neuronal stimulation, the neuron remains the major source of interstitial lactate.

Conclusions

In this review we have utilized the measurable levels and kinetic properties of GLUT1 and GLUT3 glucose transporter proteins of BBB endothelial cells, astrocytes, and neurons, along with the corresponding kinetic properties of the monocarboxylate transporters, MCT 1, 2 and 4, to successfully model brain glucose and lactate levels as well as lactate transients in response to neuronal stimulation. To the best of our knowledge this is the first working model that incorporates the cell-specific concentrations and properties of the transport proteins. In constructing this model and testing different conditions, we have revealed several important properties, and constraints, of the system. Perhaps the most vital is the appreciation of the role of the basal lamina as a post-endothelial cell “reservoir” and conduit for diffusion of glucose and metabolites directly to the interstitium. Successful modeling of relevant glucose and lactate levels requires free diffusion of glucose from the BBB endothelial cell via the adjacent basal lamina to the interstitium surrounding the neurons and astrocytes (pathway 2 of Figure 3C) and back to the serum. The other important conclusion derived from the current model is that the neuron is predicted to be responsible for the evolution of the lactate transients obtained following a neuronal stimulation and that the astrocyte may actually take up lactate under such circumstances.

Although the model presented here represents a unique contribution to the understanding of glucose and lactate metabolism in the mammalian brain, it does rely on average cellular values for the respective transporter proteins and does not address regional heterogeneity in cerebral metabolism. Such studies are clearly a goal for future exploration. However, it seems clear from these calculations that the neuron is the primary site of glucose uptake and utilization, both under steady state and stimulated conditions. Certainly this is consistent with all previous observations obtained with i*n vivo* paradigms of increased neuronal activity that demonstrate an increase in neuronal GLUT3, and BBB GLUT1 as the glucose transport accommodations to increased cerebral glucose utilization (reviewed in Vannucci et al., 1998).

Acknowledgements

This work was supported by: NIH/NINDS NS41405-01 (IAS); NIH/DK36081, NIH/DK44888, ADA 1-06-IN-04 (AC); NIH/HD PO1 HD 30704 (SJV)

References

Ackley MA, Governo RJ, Cass CE, Young JD, Baldwin SA, King AE. Control of glutamatergic neurotransmission in the rat spinal dorsal horn by the nucleoside transporter ENT1. J Physiol 2003;548:507–517. [PubMed: 12611914]

Aubert A, Costalat R. Interaction between astrocytes and neurons studied using a mathematical model of compartmentalized energy metabolism. J Cereb Blood Flow Metab 2005;25:1476–1490. [PubMed: 15931164]

Aubert A, Costalat R, Magistretti PJ, Pellerin L. Brain lactate kinetics: Modeling evidence for neuronal lactate uptake upon activation. Proc Natl Acad Sci U S A 2005;102:16448–16453. [PubMed: 16260743]

Augustin R, Carayannopoulos MO, Dowd LO, Phay JE, Moley JF, Moley KH. Identification and characterization of human glucose transporter-like protein-9 (GLUT9): alternative splicing alters trafficking. J Biol Chem 2004;279:16229–16236. [PubMed: 14739288]

Bak LK, Schousboe A, Sonnewald U, Waagepetersen HS. Glucose is necessary to maintain neurotransmitter homeostasis during synaptic activity n cultured glutamatergic neurons. J Cereb Blood Flow Metab 2006;26:1285–1297. [PubMed: 16467783]

Baker GF, Naftalin RJ. Evidence of multiple operational affinities for D-glucose inside the human erythrocyte membrane. Biochim Biophys Acta 1979;550:474–484. [PubMed: 420829]

Bergersen L, Rafiki A, Ottersen OP. Immunogold cytochemistry identifies specialized membrane domains for monocarboxylate transport in the central nervous system. Neurochem Res 2002;27:89–96. [PubMed: 11926280]

Bergersen LH, Magistretti PJ, Pellerin L. Selective postsynaptic co-localization of MCT2 with AMPA receptor GluR2/3 subunits at excitatory synapses exhibiting AMPA receptor trafficking. Cereb Cortex 2005;15:361–370. [PubMed: 15749979]

Birnbaum MJ, Haspel HC, Rosen OM. Cloning and characterization of a cDNA encoding the rat brain glucose-transporter protein. Proceedings of the National Academy of Sciences of the United States of America 1986;83:5784–5788. [PubMed: 3016720]

Blomqvist G, Gjedde A, Gutniak M, Grill V, Widen L, Stone-Elander S, Hellstrand E. Facilitated transport of glucose from blood to brain in man and the effect of moderate hypoglycaemia on cerebral glucose utilization. Eur J Nucl Med 1991;18:834–837. [PubMed: 1743207]

Brightman MW, Reese TS. Junctions between intimately apposed cell membranes in the vertebrate brain. Journal of Cell Biology 1969;40:648–677. [PubMed: 5765759]

Broer S, Broer A, Schneider HP, Stegen C, Halestrap AP, Deitmer JW. Characterization of the high-affinity monocarboxylate transporter MCT2 in Xenopus laevis oocytes. Biochem J 1999;341:529–535. [PubMed: 10417314]

Broer S, Rahman B, Pellegri G, Pellerin L, Martin JL, Verleysdonk S, Hamprecht B, Magistretti PJ. Comparison of lactate transport in astroglial cells and monocarboxylate transporter 1 (MCT 1) expressing Xenopus laevis oocytes. Expression of two different monocarboxylate transporters in astroglial cells and neurons. J Biol Chem 1997;272:30096–30102. [PubMed: 9374487]

Broer S, Schneider HP, Broer A, Rahman B, Hamprecht B, Deitmer JW. Characterization of the monocarboxylate transporter 1 expressed in Xenopus laevis oocytes by changes in cytosolic pH. Biochem J 1998;333:167–174. [PubMed: 9639576]

Brown LL, Lorden JF. Regional cerebral glucose utilization reveals widespread abnormalities in the motor system of the rat mutant dystonic. J Neurosci 1989;9:4033–4041. [PubMed: 2585066]

Carruthers A. ATP regulation of the human red cell sugar transporter. J Biol Chem 1986;261:11028–11037. [PubMed: 3733746]

Carruthers A. Facilitated diffusion of glucose. Physiological Reviews 1990;70:1135–1176. [PubMed: 2217557]

Carruthers A. Mechanisms for the facilitated diffusion of substrates across cell membranes. Biochemistry 1991;30:3898–3906. [PubMed: 2018761]

Carruthers A, Helgerson AL. The human erythrocyte sugar transporter is also a nucleotide binding protein. Biochemistry 1989;28:8337–8346. [PubMed: 2532542]

Carruthers A, Melchior DL. Asymmetric or symmetric? Cytosolic modulation of human erythrocyte hexose transfer. Biochim Biophys Acta 1983;728:254–266. [PubMed: 6681982]

Chih CP, Roberts EL Jr. Energy substrates for neurons during neural activity: a critical review of the astrocyte-neuron lactate shuttle hypothesis. J Cereb Blood Flow Metab 2003;23:1263–1281. [PubMed: 14600433]

Choi IY, Lee SP, Kim SG, Gruetter R. In vivo measurements of brain glucose transport using the reversible Michaelis-Menten model and simultaneous measurements of cerebral blood flow changes during hypoglycemia. J Cereb Blood Flow Metab 2001;21:653–663. [PubMed: 11488534]

Cloherty EK, Heard KS, Carruthers A. Human erythrocyte sugar transport is incompatible with available carrier models. Biochemistry 1996;35:10411–10421. [PubMed: 8756697]

Cloherty EK, Sultzman LA, Zottola RJ, Carruthers A. Net sugar transport is a multistep process. Evidence for cytosolic sugar binding sites in erythrocytes. Biochemistry 1995;34:15395–15406. [PubMed: 7492539]

Colville CA, Seatter MJ, Jess TJ, Gould GW, Thomas HM. Kinetic analysis of the liver-type (GLUT2) and brain-type (GLUT3) glucose transporters in Xenopus oocytes: substrate specificities and effects of transport inhibitors. Biochem J 1993;290 (Pt 3):701–706. [PubMed: 8457197]

Cornford EM, Hyman S, Pardridge WM. An electron microscopic immunogold analysis of developmental up-regulation of the blood-brain barrier GLUT1 glucose transporter. Journal of Cerebral Blood Flow & Metabolism 1993;13:841–854. [PubMed: 8360290]

Cruz NF, Adachi K, Dienel GA. Rapid efflux of lactate from cerebral cortex during K+-induced spreading cortical depression. Journal of Cerebral Blood Flow & Metabolism 1999;19:380–392. [PubMed: 10197508]

De Bruijne AW, Vreeburg H, Van Steveninck J. Kinetic analysis of L-lactate transport in human erythrocytes via the monocarboxylate-specific carrier system. Biochim Biophys Acta 1983;732:562–568. [PubMed: 6871216]

de Graaf RA, Pan JW, Telang F, Lee JH, Brown P, Novotny EJ, Hetherington HP, Rothman DL. Differentiation of glucose transport in human brain gray and white matter. J Cereb Blood Flow Metab 2001;21:483–492. [PubMed: 11333358]

Deuticke B. Monocarboxylate transport in erythrocytes. J Membr Biol 1982;70:89–103. [PubMed: 6764785]

Deuticke B. Monocarboxylate transport in red blood cells: kinetics and chemical modification. Methods Enzymol 1989;173:300–329. [PubMed: 2674614]

Dick AP, Harik SI, Klip A, Walker DM. Identification and characterization of the glucose transporter of the blood-brain barrier by cytochalasin B binding and immunological reactivity. Proceedings of the National Academy of Sciences of the United States of America 1984;81:7233–7237. [PubMed: 6150484]

Dienel GA, Cruz NF. Neighborly interactions of metabolically-activated astrocytes in vivo. Neurochem Int 2003;43:339–354. [PubMed: 12742078]

Dimmer KS, Friedrich B, Lang F, Deitmer JW, Broer S. The low-affinity monocarboxylate transporter MCT4 is adapted to the export of lactate in highly glycolytic cells. Biochem J 2000;350:219–227. [PubMed: 10926847][Record as supplied by publisher]

Doege H, Bocianski A, Joost HG, Schurmann A. Activity and genomic organization of human glucose transporter 9 (GLUT9), a novel member of the family of sugar-transport facilitators predominantly expressed in brain and leucocytes. Biochem J 2000;350:771–776. [PubMed: 10970791][Record as supplied by publisher]

Dringen R, Peters H, Wiesinger H, Hamprecht B. Lactate transport in cultured glial cells. Dev Neurosci 1995;17:63–69. [PubMed: 7555739]

Dubinsky WP, Racker E. The mechanism of lactate transport in human erythrocytes. J Membr Biol 1978;44:25–36. [PubMed: 32398]

Duelli R, Kuschinsky W. Brain glucose transporters: relationship to local energy demand. News Physiol Sci 2001;16:71–76. [PubMed: 11390952]

Dwyer DS, Vannucci SJ, Simpson IA. Expression, regulation, and functional role of glucose transporters (GLUTs) in brain. Int Rev Neurobiol 2002;51:159–188. [PubMed: 12420359]

Farrell CL, Pardridge WM. Blood-brain barrier glucose transporter is asymmetrically distributed on brain capillary endothelial lumenal and ablumenal membranes: an electron microscopic immunogold study. Proceedings of the National Academy of Sciences of the United States of America 1991;88:5779–5783. [PubMed: 2062858]

Fillenz M. The role of lactate in brain metabolism. Neurochem Int 2005;47:413–417. [PubMed: 16039756]

Fox PT, Raichle ME. Focal physiological uncoupling of cerebral blood flow and oxidative metabolism during somatosensory stimulation in human subjects. Proc Natl Acad Sci U S A 1986;83:1140–1144. [PubMed: 3485282]

Fox PT, Raichle ME, Mintun MA, Dence C. Nonoxidative glucose consumption during focal physiologic neural activity. Science 1988;241:462–464. [PubMed: 3260686]

Gerhart DZ, Broderius MA, Borson ND, Drewes LR. Neurons and microvessels express the brain glucose transporter protein GLUT3. Proceedings of the National Academy of Sciences of the United States of America 1992;89:733–737. [PubMed: 1731347]

Gerhart DZ, Enerson BE, Zhdankina OY, Leino RL, Drewes LR. Expression of monocarboxylate transporter MCT1 by brain endothelium and glia in adult and suckling rats. American Journal of Physiology 1997;273:E207–213. [PubMed: 9252498]

Gerhart DZ, Enerson BE, Zhdankina OY, Leino RL, Drewes LR. Expression of the monocarboxylate transporter MCT2 by rat brain glia. Glia 1998;22:272–281. [PubMed: 9482213]

Gerhart DZ, Leino RL, Taylor WE, Borson ND, Drewes LR. GLUT1 and GLUT3 gene expression in gerbil brain following brief ischemia: an in situ hybridization study. Brain Research Molecular Brain Research 1994;25:313–322. [PubMed: 7808230]

Gerhart DZ, LeVasseur RJ, Broderius MA, Drewes LR. Glucose transporter localization in brain using light and electron immunocytochemistry. Journal of Neuroscience Research 1989;22:464–472. [PubMed: 2668543]

Gjedde A. Rapid steady-state analysis of blood-brain glucose transfer in the rat. Acta Physiol Scand 1980;108:331–339. [PubMed: 6998256]

Gjedde A, Marrett S. Glycolysis in neurons, not astrocytes, delays oxidative metabolism of human visual cortex during sustained checkerboard stimulation in vivo. J Cereb Blood Flow Metab 2001;21:1384–1392. [PubMed: 11740199]

Gjedde A, Marrett S, Vafaee M. Oxidative and nonoxidative metabolism of excited neurons and astrocytes. J Cereb Blood Flow Metab 2002;22:1–14. [PubMed: 11807388]

Gorga FR, Lienhard GE. Changes in the intrinsic fluorescence of the human erythrocyte monosaccharide transporter upon ligand binding. Biochemistry 1982;21:1905–1908. [PubMed: 7200802]

Gruetter R, Ugurbil K, Seaquist ER. Steady-state cerebral glucose concentrations and transport in the human brain. J Neurochem 1998;70:397–408. [PubMed: 9422387]

Halestrap AP, Meredith D. The SLC16 gene family-from monocarboxylate transporters (MCTs) to aromatic amino acid transporters and beyond. Pflugers Arch 2004;447:619–628. [PubMed: 12739169]

Halestrap AP, Price NT. The proton-linked monocarboxylate transporter (MCT) family: structure, function and regulation. Biochemical Journal 1999;343:281–299. [PubMed: 10510291]

Hanu R, McKenna M, O'Neill A, Resneck WG, Bloch RJ. Monocarboxylic acid transporters, MCT1 and MCT2, in cortical astrocytes in vitro and in vivo. Am J Physiol Cell Physiol 2000;278:C921–930. [PubMed: 10794666]

Harik SI, Kalaria RN, Andersson L, Lundahl P, Perry G. Immunocytochemical localization of the erythroid glucose transporter: abundance in tissues with barrier functions. Journal of Neuroscience 1990;10:3862–3872. [PubMed: 2269888]

Hawkins RA, Biebuyck JF. Ketone bodies are selectively used by individual brain regions. Science 1979;205:325–327. [PubMed: 451608]

Hebert DN, Carruthers A. Uniporters and anion antiporters. Curr Opin Cell Biol 1991;3:702–709. [PubMed: 1663376]

Helgerson AL, Hebert DN, Naderi S, Carruthers A. Characterization of two independent modes of action of ATP on human erythrocyte sugar transport. Biochemistry 1989;28:6410–6417. [PubMed: 2506926]

Hertz L. The astrocyte-neuron lactate shuttle: a challenge of a challenge. J Cereb Blood Flow Metab 2004;24:1241–1248. [PubMed: 15545919]

Hertz L, Dienel GA. Lactate transport and transporters: general principles and functional roles in brain cells. J Neurosci Res 2005;79:11–18. [PubMed: 15586354]

Hrabetova S, Nicholson C. Contribution of dead-space microdomains to tortuosity of brain extracellular space. Neurochem Int 2004;45:467–477. [PubMed: 15186912]

Hu Y, Wilson GS. A temporary local energy pool coupled to neuronal activity: fluctuations of extracellular lactate levels in rat brain monitored with rapid-response enzyme-based sensor. J Neurochem 1997;69:1484–1490. [PubMed: 9326277]

Itoh Y, Esaki T, Kaneshige M, Suzuki H, Cook M, Sokoloff L, Cheng SY, Nunez J. Brain glucose utilization in mice with a targeted mutation in the thyroid hormone alpha or beta receptor gene. Proc Natl Acad Sci U S A 2001;98:9913–9918. [PubMed: 11481455]

Jennings ML, Adams-Lackey M. A rabbit erythrocyte membrane protein associated with L-lactate transport. J Biol Chem 1982;257:12866–12871. [PubMed: 7130184]

Jones DA, Ros J, Landolt H, Fillenz M, Boutelle MG. Dynamic changes in glucose and lactate in the cortex of the freely moving rat monitored using microdialysis. J Neurochem 2000;75:1703–1708. [PubMed: 10987853]

Joost HG, Thorens B. The extended GLUT-family of sugar/polyol transport facilitators: nomenclature, sequence characteristics, and potential function of its novel members (review). Mol Membr Biol 2001;18:247–256. [PubMed: 11780753]

Kalaria RN, Gravina SA, Schmidley JW, Perry G, Harik SI. The glucose transporter of the human brain and blood-brain barrier. Annals of Neurology 1988;24:757–764. [PubMed: 3207358]

Karlish SJD, Lieb WR, Ram D, Stein WD. Kinetic Parameters of glucose efflux from human red blood cells under zero-trans conditions. Biochim Biophys Acta 1972;255:126–132. [PubMed: 5010989]

Kasischke KA, Vishwasrao HD, Fisher PJ, Zipfel WR, Webb WW. Neural activity triggers neuronal oxidative metabolism followed by astrocytic glycolysis. Science 2004;305:99–103. [PubMed: 15232110]

Keller K, Lange K, Malkewitz J. Glucose transporter in plasma membranes of cultured neural cells, as characterized by cytochalasin B binding. J Neurochem 1986;47:1394–1398. [PubMed: 3760868]

Kimelberg HK. The role of hypotheses in current research, illustrated by hypotheses on the possible role of astrocytes in energy metabolism and cerebral blood flow: from Newton to now. J Cereb Blood Flow Metab 2004;24:1235–1239. [PubMed: 15545917]

Koehler-Stec EM, Simpson IA, Vannucci SJ, Landschulz KT, Landschulz WH. Monocarboxylate transporter expression in mouse brain. American Journal of Physiology 1998;275:E516–524. [PubMed: 9725820]

Korf J. Is brain lactate metabolized immediately after neuronal activity through the oxidative pathway? J Cereb Blood Flow Metab 2006;26:1584–1586. [PubMed: 16639423]

Lee WH, Bondy CA. Ischemic injury induces brain glucose transporter gene expression. Endocrinology 1993;133:2540–2544. [PubMed: 8243275]

Leegsma-Vogt G, van der Werf S, Venema K, Korf J. Modeling cerebral arteriovenous lactate kinetics after intravenous lactate infusion in the rat. J Cereb Blood Flow Metab 2004;24:1071–1080. [PubMed: 15529007]

Leegsma-Vogt G, Venema K, Korf J. Evidence for a lactate pool in the rat brain that is not used as an energy supply under normoglycemic conditions. J Cereb Blood Flow Metab 2003;23:933–941. [PubMed: 12902837]

Leeks DR, Halestrap AP. Chloride-independent transport of pyruvate and lactate across the erythrocyte membrane [proceedings]. Biochem Soc Trans 1978;6:1363–1366. [PubMed: 744429]

Leino RL, Gerhart DZ, Drewes LR. Monocarboxylate transporter (MCT1) abundance in brains of suckling and adult rats: a quantitative electron microscopic immunogold study. Brain Research Developmental Brain Research 1999;113:47–54. [PubMed: 10064873]

Levine KB, Cloherty EK, Fidyk NJ, Carruthers A. Structural and physiologic determinants of human erythrocyte sugar transport regulation by adenosine triphosphate. Biochemistry 1998;37:12221–12232. [PubMed: 9724536]

Leybaert L. Neurobarrier coupling in the brain: a partner of neurovascular and neurometabolic coupling? J Cereb Blood Flow Metab 2005;25:2–16. [PubMed: 15678108]

Lieb WR, Stein WD. Carrier and non–carrier models for sugar transport in the human red blood cell. Biochim Biophys Acta 1972;265:187–207. [PubMed: 4555470]

Lin RY, Vera JC, Chaganti RS, Golde DW. Human monocarboxylate transporter 2 (MCT2) is a high affinity pyruvate transporter. J Biol Chem 1998;273:28959–28965. [PubMed: 9786900]

Loaiza A, Porras OH, Barros LF. Glutamate triggers rapid glucose transport stimulation in astrocytes as evidenced by real-time confocal microscopy. J Neurosci 2003;23:7337–7342. [PubMed: 12917367]

Lowe AG, Walmsley AR. The kinetics of glucose transport in human red blood cells. Biochimica et Biophysica Acta 1986;857:146–154. [PubMed: 3707948]

Magistretti PJ, Pellerin L. Metabolic coupling during activation. A cellular view. Adv Exp Med Biol 1997;413:161–166. [PubMed: 9238497]

Magistretti PJ, Pellerin L. Astrocytes Couple Synaptic Activity to Glucose Utilization in the Brain. News Physiol Sci 1999;14:177–182. [PubMed: 11390847]

Magistretti PJ, Pellerin L, Rothman DL, Shulman RG. Energy on demand. Science 1999;283:496–497. [PubMed: 9988650]

Maher F, Davies-Hill TM, Simpson IA. Substrate specificity and kinetic parameters of GLUT3 in rat cerebellar granule neurons. Biochemical Journal 1996;315:827–831. [PubMed: 8645164]

Maher F, Simpson IA. The GLUT3 glucose transporter is the predominant isoform in primary cultured neurons: assessment by biosynthetic and photoaffinity labelling. Biochemical Journal 1994;301:379–384. [PubMed: 8042980]

Maher F, Davies-Hill T, Lysko P, Henneberry RC, Simpson IA. Expression of two glucose transporter, GLUT1 and GLUT3 in cultured cerebellar neurons: Evidence for neuron specific expression of GLUT3. Mol and Cell Neurosci 1991;2:351–360.

Maher F, Vannucci S, Takeda J, Simpson IA. Expression of mouse-GLUT3 and human-GLUT3 glucose transporter proteins in brain. Biochemical & Biophysical Research Communications 1992;182:703–711. [PubMed: 1734877]

Maher F, Vannucci SJ, Simpson IA. Glucose transporter proteins in brain. FASEB Journal 1994;8:1003–1011. [PubMed: 7926364]

Manning Fox JE, Meredith D, Halestrap AP. Characterisation of human monocarboxylate transporter 4 substantiates its role in lactic acid efflux from skeletal muscle. J Physiol 2000;529(Pt 2):285–293. [PubMed: 11101640]

McCall AL, Van Bueren AM, Moholt-Siebert M, Cherry NJ, Woodward WR. Immunohistochemical localization of the neuron-specific glucose transporter (GLUT3) to neuropil in adult rat brain. Brain Research 1994;659:292–297. [PubMed: 7820678]

McKenna MC, Tildon JT, Stevenson JH, Hopkins IB, Huang X, Couto R. Lactate transport by cortical synaptosomes from adult rat brain: characterization of kinetics and inhibitor specificity. Dev Neurosci 1998;20:300–309. [PubMed: 9778566]

Miller DM. The kinetics of selective biological transport. IV. Assessment of three carrier systems using the erythrocyte-monosaccharide transport data. Biophys J 1968;8:1339–1352. [PubMed: 5696216]

Mueckler M, Caruso C, Baldwin SA, Panico M, Blench I, Morris HR, Allard WJ, Lienhard GE, Lodish HF. Sequence and structure of a human glucose transporter. Science 1985;229:941–945. [PubMed: 3839598]

Nagamatsu S, Kornhauser JM, Burant CF, Seino S, Mayo KE, Bell GI. Glucose transporter expression in brain. cDNA sequence of mouse GLUT3, the brain facilitative glucose transporter isoform, and identification of sites of expression by in situ hybridization. Journal of Biological Chemistry 1992;267:467–472. [PubMed: 1730609]

Nagamatsu S, Sawa H, Kamada K, Nakamichi Y, Yoshimoto K, Hoshino T. Neuron-specific glucose transporter (NSGT): CNS distribution of GLUT3 rat glucose transporter (RGT3) in rat central neurons. FEBS Letters 1993;334:289–295. [PubMed: 8243635]

Nedergaard M, Goldman SA. Carrier-mediated transport of lactic acid in cultured neurons and astrocytes. Am J Physiol 1993;265:R282–289. [PubMed: 8368382]

Nehlig A, Pereira de Vasconcelos A. Glucose and ketone body utilization by the brain of neonatal rats. Prog Neurobiol 1993;40:163–221. [PubMed: 8430212]

Nicholson C. Factors governing diffusing molecular signals in brain extracellular space. J Neural Transm 2005;112:29–44. [PubMed: 15372328]

Pattillo RE, Gladden LB. Red blood cell lactate transport in sickle disease and sickle cell trait. J Appl Physiol 2005;99:822–827. [PubMed: 15890755]

Pellerin L, Magistretti PJ. Glutamate uptake into astrocytes stimulates aerobic glycolysis: a mechanism coupling neuronal activity to glucose utilization. Proc Natl Acad Sci U S A 1994;91:10625–10629. [PubMed: 7938003]

Pellerin L, Magistretti PJ. Food for thought: challenging the dogmas. J Cereb Blood Flow Metab 2003;23:1282–1286. [PubMed: 14600434]

Pellerin L, Pellegri G, Martin JL, Magistretti PJ. Expression of monocarboxylate transporter mRNAs in mouse brain: support for a distinct role of lactate as an energy substrate for the neonatal vs. adult brain. Proceedings of the National Academy of Sciences of the United States of America 1998;95:3990–3995. [PubMed: 9520480]

Philp NJ, Yoon H, Lombardi L. Mouse MCT3 gene is expressed preferentially in retinal pigment and choroid plexus epithelia. Am J Physiol Cell Physiol 2001;280:C1319–1326. [PubMed: 11287345]

Pierre K, Magistretti PJ, Pellerin L. MCT2 is a major neuronal monocarboxylate transporter in the adult mouse brain. J Cereb Blood Flow Metab 2002;22:586–595. [PubMed: 11973431]

Pierre K, Pellerin L. Monocarboxylate transporters in the central nervous system: distribution, regulation and function. J Neurochem 2005;94:1–14. [PubMed: 15953344]

Pierre K, Pellerin L, Debernardi R, Riederer BM, Magistretti PJ. Cell-specific localization of monocarboxylate transporters, MCT1 and MCT2, in the adult mouse brain revealed by double immunohistochemical labeling and confocal microscopy. Neuroscience 2000;100:617–627. [PubMed: 11098125]

Poole RC, Halestrap AP. Transport of lactate and other monocarboxylates across mammalian plasma membranes. Am J Physiol 1993;264:C761–782. [PubMed: 8476015]

Porras OH, Loaiza A, Barros LF. Glutamate mediates acute glucose transport inhibition in hippocampal neurons. J Neurosci 2004;24:9669–9673. [PubMed: 15509754]

Prichard J, Rothman D, Novotny E, Petroff O, Kuwabara T, Avison M, Howseman A, Hanstock C, Shulman R. Lactate rise detected by 1H NMR in human visual cortex during physiologic stimulation. Proc Natl Acad Sci U S A 1991;88:5829–5831. [PubMed: 2062861]

Qutub AA, Hunt CA. Glucose transport to the brain: a systems model. Brain Res Brain Res Rev 2005;49:595–617. [PubMed: 16269321]

Rafiki A, Boulland JL, Halestrap AP, Ottersen OP, Bergersen L. Highly differential expression of the monocarboxylate transporters MCT2 and MCT4 in the developing rat brain. Neuroscience 2003;122:677–688. [PubMed: 14622911]

Rumsey SC, Kwon O, Xu GW, Burant CF, Simpson I, Levine M. Glucose transporter isoforms GLUT1 and GLUT3 transport dehydroascorbic acid. Journal of Biological Chemistry 1997;272:18982–18989. [PubMed: 9228080]

Saier MH Jr, Beatty JT, Goffeau A, Harley KT, Heijne WH, Huang SC, Jack DL, Jahn PS, Lew K, Liu J, Pao SS, Paulsen IT, Tseng TT, Virk PS. The major facilitator superfamily. J Mol Microbiol Biotechnol 1999;1:257–279. [PubMed: 10943556]

Siesjo, BK. Brain Energy Metalolism. New York: John Wiley & Sons; 1978.

Simpson IA, Appel NM, Hokari M, Oki J, Holman GD, Maher F, Koehler-Stec EM, Vannucci SJ, Smith QR. Blood-brain barrier glucose transporter: effects of hypo- and hyperglycemia revisited. Journal of Neurochemistry 1999;72:238–247. [PubMed: 9886075]

Simpson IA, Davies P. Reduced glucose transporter concentrations in brains of patients with Alzheimer's disease. Ann Neurol 1994;36:800–801. [PubMed: 7979229]

Simpson IA, Vannucci SJ, DeJoseph MR, Hawkins RA. Glucose transporter asymmetries in the bovine blood-brain barrier. J Biol Chem 2001;276:12725–12729. [PubMed: 11278779]

Sivitz W, DeSautel S, Walker PS, Pessin JE. Regulation of the glucose transporter in developing rat brain. Endocrinology 1989;124:1875–1880. [PubMed: 2924729]

Sokoloff, L. Circulation and energy metabolism in the brain. Boston: Little Brown and Company; 1976.

Sokoloff L, Reivich M, Kennedy C, Des Rosiers MH, Patlak CS, Pettigrew KD, Sakurada O, Shinohara M. The [14C]deoxyglucose method for the measurement of local cerebral glucose utilization: theory, procedure, and normal values in the conscious and anesthetized albino rat. Journal of Neurochemistry 1977;28:897–916. [PubMed: 864466]

Sorra KE, Harris KM. Overview on the structure, composition, function, development, and plasticity of hippocampal dendritic spines. Hippocampus 2000;10:501–511. [PubMed: 11075821]

Stein, WB. Transport and diffusion across cell membranes. Academic Press; New York: 1986a.

Stein, WD. Transport and diffusion across cell membranes. Academic Press; New York: 1986b.

Tao A, Tao L, Nicholson C. Cell cavities increase tortuosity in brain extracellular space. J Theor Biol 2005;234:525–536. [PubMed: 15808873]

Tao L, Masri D, Hrabetova S, Nicholson C. Light scattering in rat neocortical slices differs during spreading depression and ischemia. Brain Res 2002;952:290–300. [PubMed: 12376191]

Tao L, Nicholson C. Maximum geometrical hindrance to diffusion in brain extracellular space surrounding uniformly spaced convex cells. J Theor Biol 2004;229:59–68. [PubMed: 15178185]

Tildon JT, McKenna MC, Stevenson J, Couto R. Transport of L-lactate by cultured rat brain astrocytes. Neurochem Res 1993;18:177–184. [PubMed: 8474559]

Tsacopoulos M, Magistretti PJ. Metabolic coupling between glia and neurons. Journal of Neuroscience 1996;16:877–885. [PubMed: 8558256]

Uldry M, Thorens B. The SLC2 family of facilitated hexose and polyol transporters. Pflugers Arch 2004;447:480–489. [PubMed: 12750891]

Vannucci SJ. Developmental expression of GLUT1 and GLUT3 glucose transporters in rat brain. Journal of Neurochemistry 1994;62:240–246. [PubMed: 8263524]

Vannucci SJ, Maher F, Simpson IA. Glucose transporter proteins in brain: delivery of glucose to neurons and glia. Glia 1997;21:2–21. [PubMed: 9298843]

Vannucci SJ, Simpson IA. Developmental switch in brain nutrient transporter expression in the rat. Am J Physiol Endocrinol Metab 2003;285:E1127–1134. [PubMed: 14534079]

Vannucci SJ, Willing LB, Vannucci RC. Developmental expression of glucose transporters, GLUT1 and GLUT3, in postnatal rat brain. Advances in Experimental Medicine & Biology 1993;331:3–7. [PubMed: 8333346]

Weber, TM.; Joost, HG.; Simpson, IA.; Cushman, SW. Methods of assessment of glucose transport activity and the number of glucsoe transporters in isolated rat adipose cells and membrane fractions. In: Kahn, CR.; Harrison, LC., editors. The Insulin Receptor. New York, NY: Alan R. Liss; 1988. p. 171-187.

Wheeler TJ, Simpson IA, Sogin DC, Hinkle PC, Cushman SW. Detection of the rat adipose cell glucose transporter with antibody against the human red cell glucose transporter. Biochemical & Biophysical Research Communications 1982;105:89–95. [PubMed: 7046746]

Whitesell RR, Ward M, McCall AL, Granner DK, May JM. Coupled glucose transport and metabolism in cultured neuronal cells: determination of the rate-limiting step. J Cereb Blood Flow Metab 1995;15:814–826. [PubMed: 7673374]

Widdas WF. The asymmetry of the hexose transfer system in the human red cell membrane. Curr Top Memb Transp 1980;14:165–223.

Wilson JE. Isozymes of mammalian hexokinase: structure, subcellular localization and metabolic function. J Exp Biol 2003;206:2049–2057. [PubMed: 12756287]

Wood IS, Trayhurn P. Glucose transporters (GLUT and SGLT): expanded families of sugar transport proteins. Br J Nutr 2003;89:3–9. [PubMed: 12568659]

Appendix Table 1

Model compartments, inflows/outflows and starting conditions

The compartments of Figure 4 (endothelium (e), basal lamina (bl), astrocyte (a), interstitium (int) and neuron (n)) are subdivided into glucose and lactate compartments (e.g. Glc^e and Lac^e). The inflows/outflows (J) cross-reference to Figure 4 through their assigned number. For example net flow of glucose into the endothelium is given by J1–J2 where J1 represents GLUT1-mediated net glucose movement from serum to endothelium (Fig 4) and J2 is net sugar movement from endothelium to interstitium (Fig 4). Starting conditions for simulations assumed that each compartment was glucose- and lactate-free.

Glucose Compartments & inflow outflow	Lactate Compartments & inflow outflow
$Glc^e = [Glc]_{Endothelium}. V^e$ $d/dt\ (Glc^e) = + J1 - J2$	$Lac^e = [Lactate]_{Endothelium}. V^e$ $d/dt\ (Lac^e) = + J11 - J12$
$Glc^{bl} = [Glc]_{BasalLamina}. V^{bl}$ $d/dt\ (Glc^{bl}) = + J2 - J3 - J4$	$Lac^{bl} = [Lactate]_{BasalLamina}. V^{bl}$ $d/dt\ (Lac^{bl}) = + J12 - J13 - J14$
$Glc^a = [Glc]_{Astrocyte}. V^a$ $d/dt\ (Glc^a) = + J3 - J5 - J7 - J8$	$Lac^a = [Lactate]_{Astrocyte}. V^a$ $d/dt\ (Lac^a) = J7 + J13 - J15 - J17$
$Glc^{int} = [Glc]_{Interstitium}. V^{int}$ $d/dt\ (Glc^{int}) = + J4 + J5 - J6$	$Lac^{int} = [Lactate]_{Interstitium}. V^{int}$ $d/dt\ (Lac^{int}) = + J14 + J15 - J16$
$Glc^n = [Glc]_{Neuron}. V^n$ $d/dt\ (Glc^n) = + J6 - J9 - J10$	$Lac^n = [Lactate]_{Neuron}. V^n$ $d/dt\ (Lac^n) = + J9 + J16 - J18$

Appendix Table 2

Flow equations

The flow (J) cross-references to Figure 4 through the assigned number. For example net flow of glucose from serum to endothelium is given by J1 (Fig 4). The corresponding steady-state carrier-mediated transport equation describing a specific flow is indicated in column 2. The parameters (meaning and values) are described in Appendix Table 3.

flow	Appendix Table 2 flow equations		
J1	$$\frac{Glc^s(K+\frac{Glc^e}{V^e})-\frac{Glc^e}{V^e}(K+Glc^s)}{K^2R_{oo}+KR_{oi}Glc^s+KR_{io}\frac{Glc^e}{V^e}+R_{ee}\frac{Glc^e}{V^e}Glc^s}$$		
J2	$$\frac{\frac{Glc^e}{V^e}(K+\frac{Glc^{bl}}{V^{bl}})-\frac{Glc^{bl}}{V^{bl}}(K+\frac{Glc^e}{V^e})}{K^2R_{oo}+KR_{oi}\frac{Glc^{bl}}{V^{bl}}+KR_{io}\frac{Glc^e}{V^e}+R_{ee}\frac{Glc^{bl}}{V^{bl}}\frac{Glc^e}{V^e}}$$		
J3	$$\frac{\frac{Glc^{bl}}{V^{bl}}({}^aK+\frac{Glc^a}{V^a})-\frac{Glc^a}{V^a}({}^aK+\frac{Glc^{bl}}{V^{bl}})}{{}^aK^2\,{}^{bla}R_{oo}+{}^aK\,{}^{bla}R_{oi}\frac{Glc^{bl}}{V^{bl}}+{}^aK\,{}^{bla}R_{io}\frac{Glc^a}{V^a}+{}^{bla}R_{ee}\frac{Glc^{bl}}{V^{bl}}\frac{Glc^e}{V^e}}$$		
J4	$$\frac{Glc^{bl}}{V^{bl}}k_{app}(1x10^{15})-\frac{Glc^{int}}{V^{int}}k_{app}(1x10^{15})$$		
J5	$$\frac{\frac{Glc^a}{V^a}({}^aK+\frac{Glc^{int}}{V^{int}})-\frac{Glc^{int}}{V^{int}}({}^aK+\frac{Glc^a}{V^a})}{{}^aK^2\,{}^{int a}R_{oo}+{}^aK\,{}^{int a}R_{oi}\frac{Glc^{int}}{V^{int}}+{}^aK\,{}^{int a}R_{io}\frac{Glc^a}{V^a}+{}^{int a}R_{ee}\frac{Glc^{int}}{V^{int}}\frac{Glc^a}{V^a}}$$		
J6	$$\frac{\frac{Glc^{int}}{V^{int}}({}^nK+\frac{Glc^n}{V^n})-\frac{Glc^n}{V^n}({}^nK+\frac{Glc^{int}}{V^{int}})}{{}^nK^2\,{}^nR_{oo}+{}^nK\,{}^nR_{oi}\frac{Glc^{int}}{V^{int}}+{}^nK\,{}^nR_{io}\frac{Glc^n}{V^n}+{}^nR_{ee}\frac{Glc^{int}}{V^{int}}\frac{Glc^n}{V^n}}$$		
J7	$$\frac{11/12\,{}^aV_h\frac{Glc^a}{V^a}}{K_h+\frac{Glc^a}{V^a}}$$	J8	$$\frac{1/12\,{}^aV_h\frac{Glc^a}{V^a}}{K_h+\frac{Glc^a}{V^a}}$$
J9	$$\frac{11/12\frac{V^n}{V^a}\,{}^nV_h\frac{Glc^n}{V^n}}{K_h+\frac{Glc^n}{V^n}}$$	J10	$$\frac{1/12\frac{V^n}{V^a}\,{}^nV_h\frac{Glc^n}{V^n}}{K_h+\frac{Glc^n}{V^n}}$$
J11	$$\frac{Lac\,[H^+]({}^eK_L+\frac{[H^+]Lac^e}{V^e})-\frac{[H^+]Lac^e}{V^e}({}^eK_L+[H^+]Lac)}{{}^eK_L^2\,{}^{eL}R_{oo}+{}^eK_L\,{}^eR_{oi}[H^+]Lac+{}^eR_L\,{}^eR_{io}\frac{[H^+]Lac^e}{V^e}+{}^eR_{ee}\frac{[H^+]Lac^e}{V^e}}$$		
J12	$$\frac{\frac{[H^+]Lac^e}{V^e}({}^eK_L+\frac{[H^+]Lac^{bl}}{V^{bl}})-\frac{[H^+]Lac^{bl}}{V^{bl}}({}^eK_L+\frac{[H^+]Lac^e}{V^e})}{{}^eK_L^2\,{}^eR_{oo}+{}^eK_L\,{}^eR_{oi}\frac{[H^+]Lac^{bl}}{V^{bl}}+{}^eK_L\,{}^eR_{io}\frac{[H^+]Lac^e}{V^e}+{}^eR_{ee}\frac{[H^+]Lac^{bl}}{V^{bl}}\frac{[H^+]Lac^e}{V^e}}$$		
J13	$$\frac{\frac{[H^+]Lac^{bl}}{V^{bl}}({}^aK_L+\frac{[H^+]Lac^a}{V^a})-\frac{[H^+]Lac^a}{V^a}({}^aK_L+\frac{[H^+]Lac^{bl}}{V^{bl}})}{{}^aK_L^2\,{}^{bla}R_{oo}+{}^aK_L\,{}^{bla}R_{oi}\frac{[H^+]Lac^{bl}}{V^{bl}}+{}^aK_L\,{}^{bla}R_{io}\frac{[H^+]Lac^a}{V^a}+{}^{bla}R_{ee}\frac{[H^+]Lac^{bl}}{V^{bl}}\frac{[H^+]Lac^a}{V^aV^a}}$$		

flow	Appendix Table 2 flow equations		
J14	$\frac{Lac^{bl}}{V^{bl}}k_{app}(1x10^{15}) - \frac{Lac^{int}}{V^{int}}k_{app}(1x10^{15})$		
J15	$\frac{[H^+]Lac^a}{V^a}({}^aK_L + \frac{[H^+]Lac^{int}}{V^{int}}) - \frac{[H^+]Lac^{int}}{V^{int}}({}^aK_L + \frac{[H^+]Lac^a}{V^a})$ / ${}^aK_L^2\ {}^{inta}_{L}R_{oo} + {}^aK_L\ {}^{inta}_{L}R_{oi}\frac{[H^+]Lac^{int}}{V^{int}} + {}^aK_L\ {}^{inta}_{L}R_{io}\frac{[H^+]Lac^a}{V^a} + {}^{inta}_{L}R_{ee}\frac{[H^+]Lac^{int}}{V^{int}}\frac{[H^+]Lac^a}{V^aV^a}$		
J16	$\frac{[H^+]Lac^{int}}{V^{int}}({}^nK_L + \frac{[H^+]Lac^n}{V^n}) - \frac{[H^+]Lac^n}{V^n}({}^nK_L + \frac{[H^+]Lac^{int}}{V^{int}})$ / ${}^nK_L^2\ {}^{n}_{L}R_{oo} + {}^nK_L\ {}^{n}_{L}R_{oi}\frac{[H^+]Lac^{int}}{V^{int}} + {}^nK_L\ {}^{n}_{L}R_{io}\frac{[H^+]Lac^n}{V^n} + {}^{n}_{L}R_{ee}\frac{[H^+]Lac^{int}}{V^{int}}\frac{[H^+]Lac^n}{V^n}$		
J17	$\frac{{}^aV_L\frac{Lac^a}{V^a}}{K_L + \frac{Lac^a}{V^a}}$	J18	$\frac{\frac{V^n}{V^a}\,{}^nV_L\frac{Lac^n}{V^n}}{K_L + \frac{Lac^n}{V^n}}$

Appendix Table 3

Definition of Model parameters

The parameters, constants and calculations used in flow simulations (Appendix Tables 1 & 2) are summarized here. For example, R_{oi} for GLUT1-mediated sugar transport into and out of the endothelium is $R_{oi} = 13 \times 10^{13}$ sec/mmol. K_m for net lactate uptake and exit are given by $K_L \cdot {}_LR_{oo}/[H^+]/{}_LR_{oi}$ and $K_L \cdot {}_LR_{oo}/[H^+]/{}_LR_{io}$ respectively.

Volumes V^e = endothelium volume=1.35×10^{-15} L V^{bl} = basal lamina volume = 1.2×10^{-15} L V^a = astrocyte volume = 22.7×10^{-15} L V^{int} = interstitium volume = 14×10^{-15} L V^n = neuron volume = 39×10^{-15} L	*Astrocyte transport of Glc and lactate* Note that the astrocyte presents two surfaces - one facing the basal lamina and one facing the interstitium. Assuming GLUT1 (and MCT1/4) is uniformly distributed across the entire cell membrane, R terms for transport in the direction basal lamina to astrocyte will be significantly greater than R terms for transport in the direction astrocyte to interstitium because less carrier contributes to the substrate flux.
Diffusion constants $D_{Glc} \approx D_{Lac}$ = self-diffusion coefficient for D-glucose and lactate in aqueous solution = 7×10^{-6} $cm^2.s^{-1}$ λ = tortuosity factor = 1.6 ϕ = average distance of diffusion = 8.5 μm k_{app} = apparent rate constant for self-diffusion of glucose in brain = $D_{Glc}/\lambda/\phi^2 = 6$ sec^{-1}	*Astrocyte Glc transport (basal lamina to astrocyte)* ${}^{bla}R_{oi} = 6.25 \times 10^{15}$ sec/mmol ${}^{bla}R_{io} = 4.75 \times 10^{15}$ sec/mmol ${}^{bla}R_{ee} = 4.75 \times 10^{15}$ sec/mmol ${}^{bla}R_{oo} = {}^{bla}R_{oi} + {}^{bla}R_{io} - {}^{bla}R_{ee}$ sec/mmol ${}^aK$ = 10 mM
Endothelial Glc transport $R_{oi} = 13 \times 10^{13}$ sec/mmol $R_{io} = 13 \times 10^{13}$ sec/mmol $R_{ee} = 13 \times 10^{13}$ sec/mmol $R_{oo} = R_{oi} + R_{io} - R_{ee}$ sec/mmol K = 10 mM	*Astrocyte Glc transport (astrocyte to interstitium)* ${}^{inta}R_{oi} = 5.2 \times 10^{14}$ sec/mmol ${}^{inta}R_{io} = 3.8 \times 10^{14}$ sec/mmol ${}^{inta}R_{ee} = 3.8 \times 10^{14}$ sec/mmol ${}^{inta}R_{oo} = {}^{inta}Roi + {}^{inta}Rio - {}^{inta}Ree$ sec/mmol ${}^aK$ = 10 mM
Neuron Glc transport ${}^nR_{oi} = 4.4 \times 10^{13}$ sec/mmol ${}^nR_{io} = 3.2 \times 10^{13}$ sec/mmol ${}^nR_{ee} = 3.2 \times 10^{13}$ sec/mmol ${}^nR_{oo} = {}^nR_{oi} + {}^nR_{io} - {}^nR_{ee}$ sec/mmol ${}^nK$ = 4 mM	*Endothelial Lactate transport* ${}^{e}_{L}R_{oi} = 2.8 \times 10^{15}$ sec / mmol ${}^{e}_{L}R_{io} = 2 \times 10^{15}$ sec / mmol ${}^{e}_{L}R_{ee} = 2 \times 10^{15}$ sec / mmol ${}^{e}_{L}R_{oo} = {}^{e}_{L}R_{oi} + {}^{e}_{L}R_{io} - {}^{e}_{L}R_{ee}$ sec / mmol ${}^eK_L = 1 \times 10^{-7}$ M, $[H^+]$= 62.5 nM
Astrocyte Lactate transport (basal lamina to astrocyte) ${}^{bla}_{L}R_{oi} = 8.25 \times 10^{14}$ sec / mmol ${}^{bla}_{L}R_{io} = 8.25 \times 10^{14}$ sec / mmol ${}^{bla}_{L}R_{ee} = 1.25 \times 10^{14}$ sec / mmol ${}^{bla}_{L}R_{oo} = {}^{bla}_{L}R_{oi} + {}^{bla}_{L}R_{io} - {}^{bla}_{L}R_{ee}$ sec / mmol ${}^aK_L = 2 \times 10^{-7}$ M, $[H^+]$= 62.5 nM	*Astrocyte Lactate transport (astrocyte to interstitium)* ${}^{inta}_{L}R_{oi} = 6.6 \times 10^{13}$ sec / mmol ${}^{inta}_{L}R_{io} = 6.6 \times 10^{13}$ sec / mmol ${}^{inta}_{L}R_{ee} = 1 \times 10^{13}$ sec / mmol ${}^{inta}_{L}R_{oo} = {}^{inta}_{L}R_{oi} + {}^{inta}_{L}R_{io} - {}^{inta}_{L}R_{ee}$ sec / mmol ${}^aK_L = 2 \times 10^{-7}$ M, $[H^+]$= 62.5 nM
Neuron Lactate transport	*Metabolic Constants* $K_h = K_m$ hexokinase for Glc = 0.045 mM

${}^{n}_{L}R_{oi} = 2.0 \times 10^{14}\ \text{sec} \Big/ \text{mmol}$ ${}^{n}_{L}R_{io} = 2 \times 10^{14}\ \text{sec} \Big/ \text{mmol}$ ${}^{n}_{L}R_{ee} = 3 \times 10^{13}\ \text{sec} \Big/ \text{mmol}$ ${}^{n}_{L}R_{oo} = {}^{n}_{L}R_{oi} + {}^{n}_{L}R_{io} - {}^{n}_{L}R_{ee}\ \text{sec} \Big/ \text{mmol}$ ${}^{n}K_{L} = 2 \times 10^{-8}$ M, $[H^{+}] = 62.5$ nM	${}^{a}V_{h}$ = astrocyte V_{max} hexokinase = GCF/${}^{ai}R_{oi}$ ${}^{n}V_{h}$ = neuron V_{max} hexokinase = GCF/3/${}^{n}R_{oi}$ GCF = 0.0495 $K_{L} = K_{m}$ lactate metabolism = 2 mM ${}^{a}V_{L}$ = astrocyte V_{max} lactate consumption = $\text{OCF} \Big/ 4 \Big/ {}^{inta}_{nL}R_{oi}$ ${}^{n}V_{L}$ = neuron V_{max} lactate consumption = $1.25\,\text{OCF} \Big/ {}^{n}_{L}R_{oi}$ OCF = 0.0975
Substrate levels Serum [Glucose] = Glc^{S} = 6 mM Serum [Lactate] = Lac = 1mM	

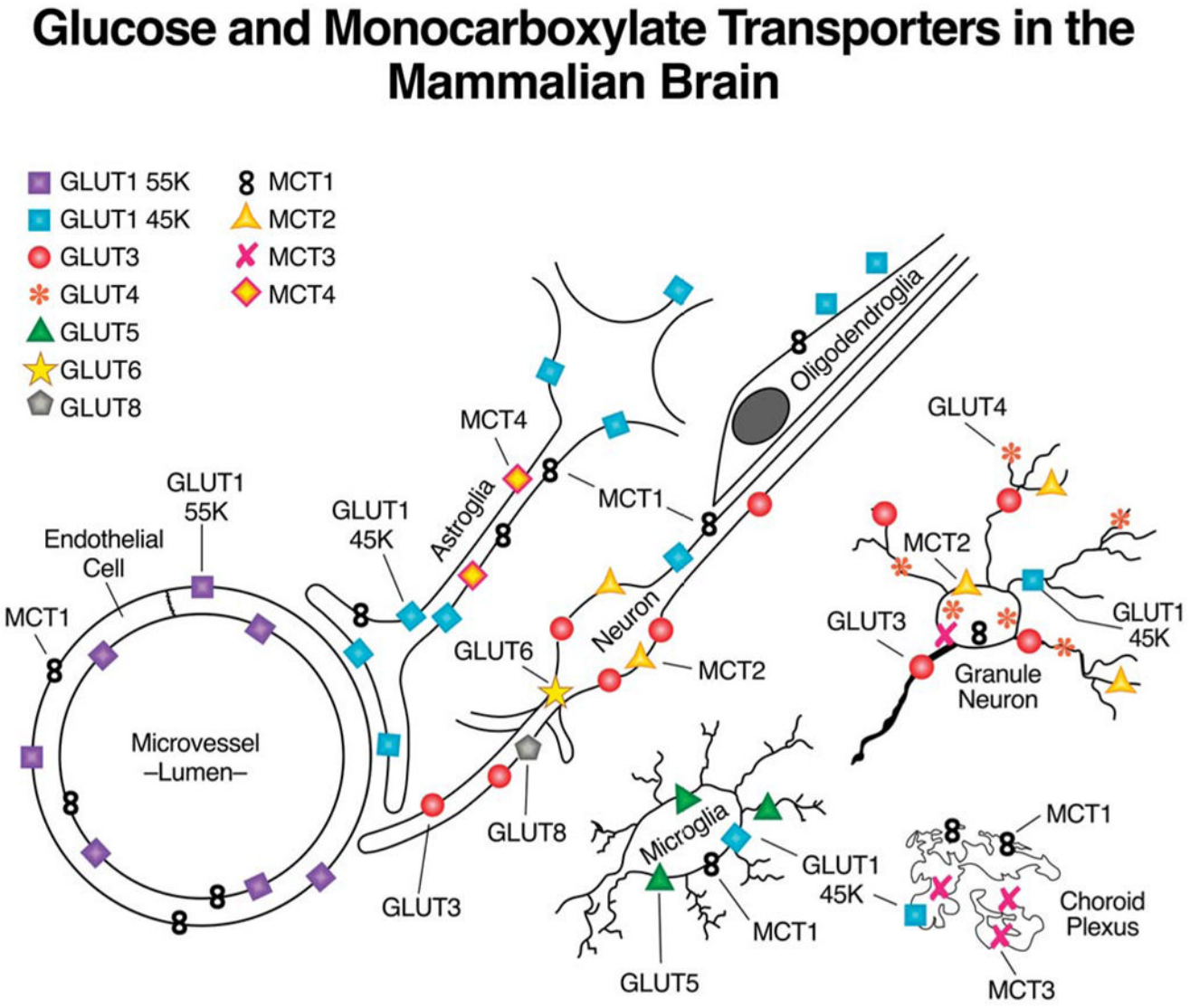

Figure 1.
A schematic representation of the cellular localization of glucose transporter (GLUTs) and monocarboxylate transporters (MCTs) in mammalian brain (McKenna et al. 2005).

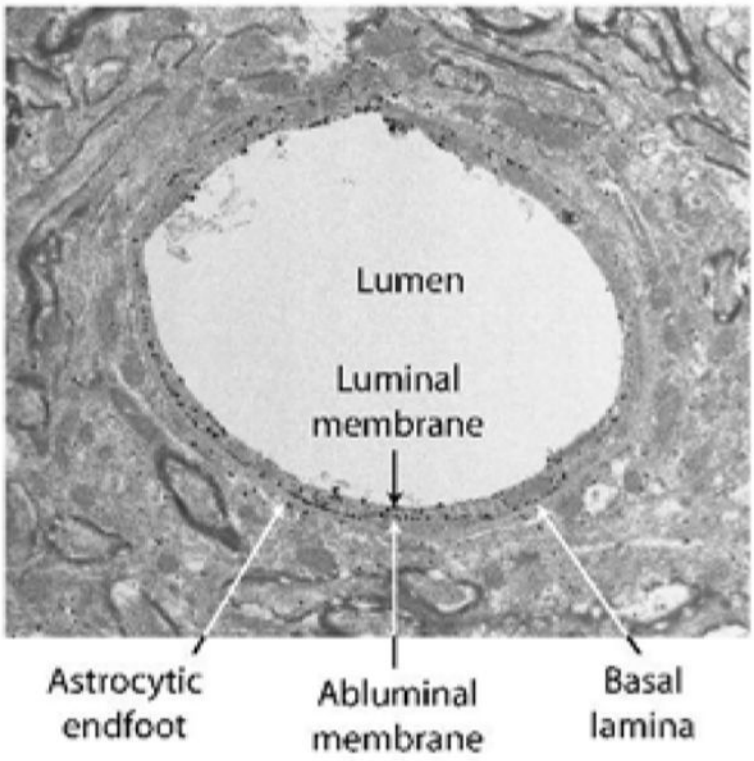

Figure 2. A representative electron micrograph illustrating the relative distribution of immunogold labeling of GLUT1 glucose transporters in endothelial cells and astrocytic endfeet

GLUT1 glucose transporters were detected by a combination of an antibody raised against purified human erythrocyte GLUT1 (Wheeler et al. 1982) and Alexa Fluronanogold Fab fragment goat anti rabbit Nanoprobe. Arrows, endothelial GLUT1; arrowheads, astrocytic GLUT1.

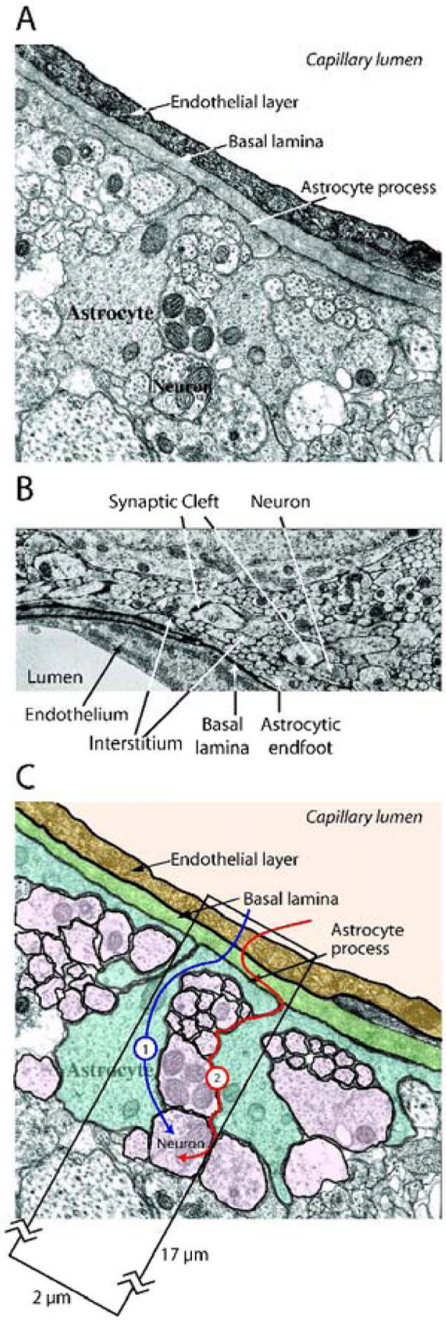

Figure 3. Electron micrograph depiction of barriers and pathways for solute delivery from serum to brain

A. A typical electron micrograph depicting endothelial cell interactions with surrounding astrocytes and neurons. Electron micrograph kindly provided by Dr. Robert Page (Hawkins et al. 2006).

B. Electron micrograph illustrating interstitial diffusion of horseradish peroxidase. Horseradish peroxidase was injected directly into the lateral ventricles of the rat and diffused throughout the interstitium, between neurons and glia (arrowheads), up to, and including, the basal lamina (arrows). Electron micrograph was kindly provided by Dr. Milton Brightman (Brightman and Reese 1969).

C. Diagrammatic representation of potential routes of glucose diffusion from blood to the neuron. Route 1 depicts glucose traversing the basal lamina whence it is transported into the astrocytic endfoot. Astrocytic glucose is either directly exported into the interstitium or is metabolized to lactate which is subsequently exported to the interstitium. Route 2 depicts the diffusion of glucose throughout the basal lamina, into the interstitium, and subsequently to the respective neurons and astrocytes.

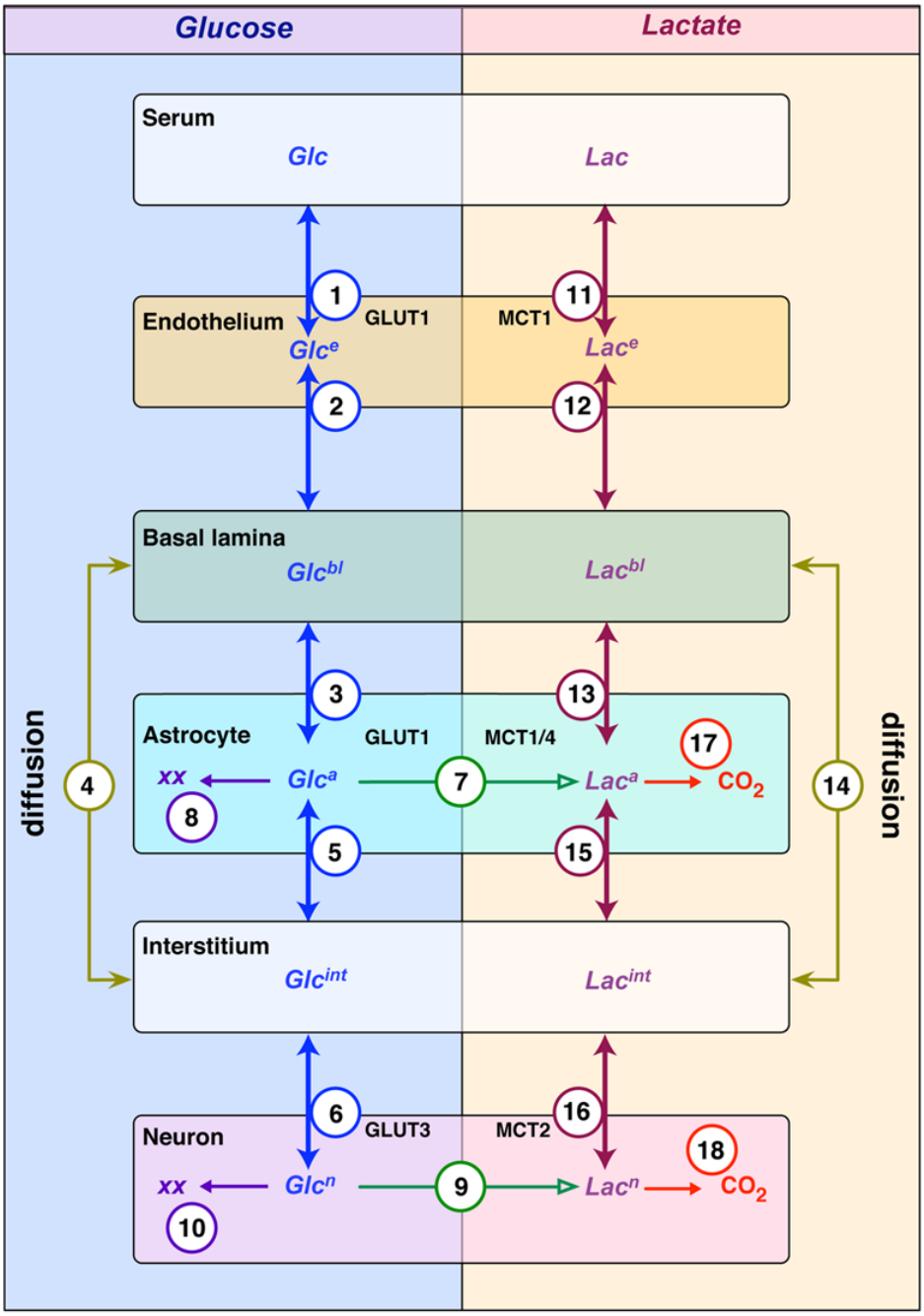

Figure 4. Compartment model for glucose transport and metabolism in mammalian brain

Glucose (Glc) and lactate distribute among 6 compartments in the brain: serum; endothelial cells; basal lamina; interstitium; astrocytes; and neurons. Glc distributions are shown on the left and lactate distributions on the right. Flows between compartments (transport is bidirectional and metabolism is unidirectional) are indicated by the arrows (double or single-headed, respectively). Each flow is assigned a number and the transport process is indicated. For example, the astrocyte shows four flows for Glc: GLUT1-mediated uptake from basal lamina (flow 3); GLUT1-mediated uptake from interstitium (flow 5); metabolic conversion to lactate (flow 7); and to other metabolites (XX) such as glycogen (flow 8). Direct flow of Glc and lactate between the basal lamina and interstitium is diffusion-mediated and is described

by flows 4 (Glc) and 14 (lactate), respectively. The number assigned to each flow is cross-referenced in Appendix Tables 1 and 2. Appendix Table 2 presents the mass transport equation describing each individual net flow and Appendix Table 3 describes each parameter contributing to each flow equation and the volume of each compartment.

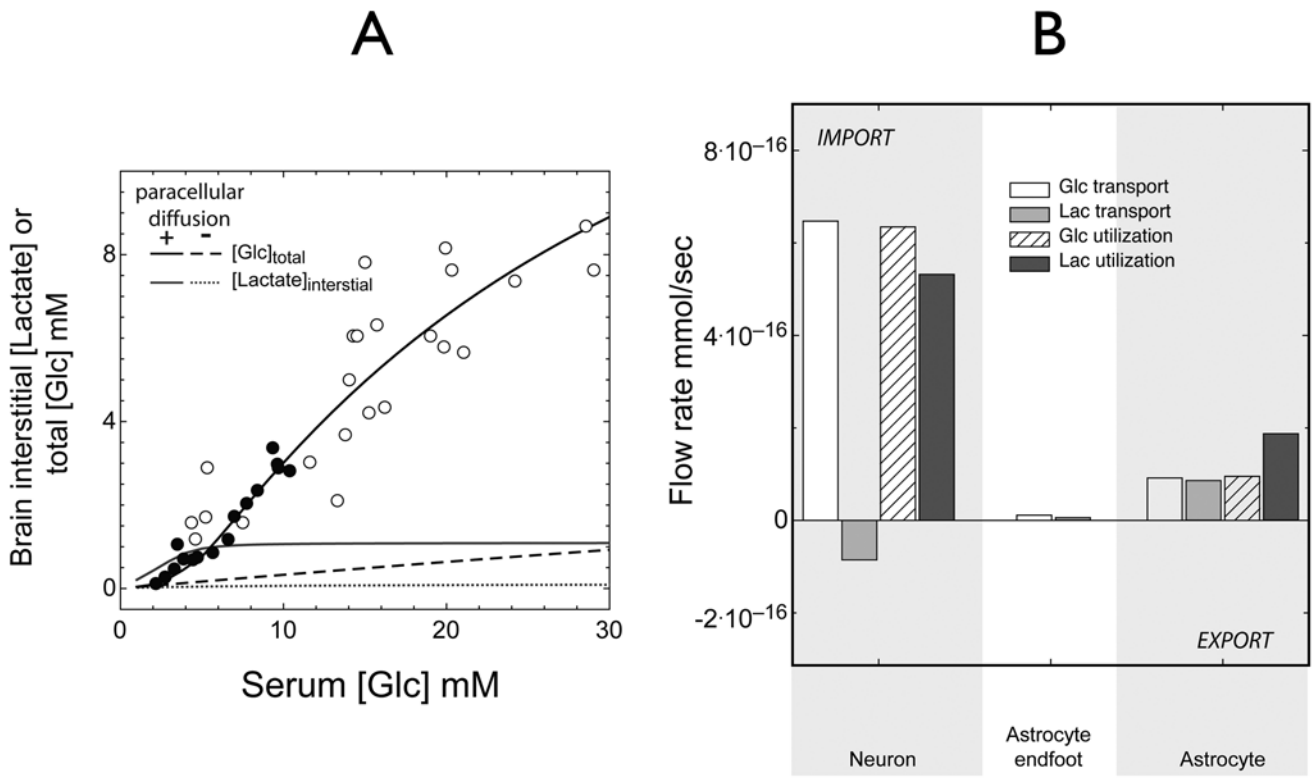

Figure 5. Simulations of basal, steady-state brain total glucose and interstitial lactate versus serum glucose

A. Brain total [Glc] (black lines) or interstitial [lactate] (blue lines) (mM) are determined as a function of serum [Glc] in mM. The circles show measurements of steady-state glucose levels in rat (filled circles) and human (open circles) brain observed at varying serum [Glc] (Choi et al. 2001; Gruetter et al. 1998) and fixed serum [lactate] (1 mM). The solid black line indicates close agreement between predicted and experimental data. When paracellular diffusion is prevented (Pathway 1, Figure 3C, dotted lines), predicted total glucose and interstitial lactate levels fall significantly.

B. Contributions to brain total [Glc] and interstitial [lactate] at 6 mM serum glucose and 1 mM serum lactate. The ordinate indicates net flux (mmol/sec) of glucose and lactate at 3 membrane sites: neuron; astrocytic endfoot; and the astrocyte/interstitium prior to stimulation. The neuron is the primary source of lactate production: 14% is exported to interstitium, the remainder is metabolized by the neuron. See Figure 8A for the origins of the lactate transients. The astrocyte imports 50% of consumed lactate from the interstitium.

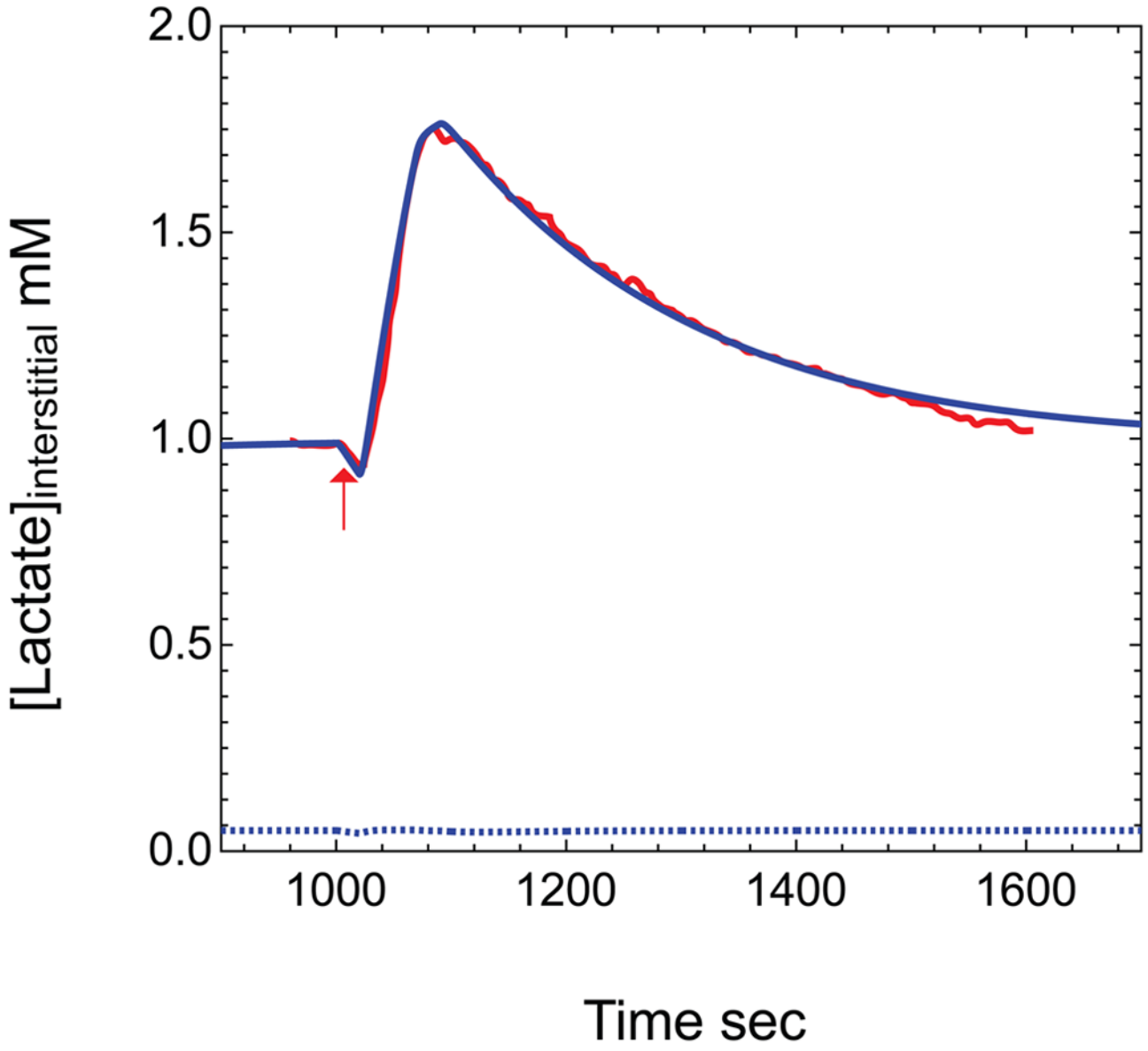

Figure 6. Lactate transients during neuronal stimulation

Data obtained from Hu and Wilson (Hu and Wilson, 1997) of extracellular measurements of lactate made during and following a short period of neuronal stimulation are shown in red. The blue curve depicts simulated brain interstitial [lactate] (mM) obtained upon applying the model presented in Figure 4 with parameters summarized in Appendix Table 3. Neuronal and astrocytic lactate oxidation were simulated to undergo a 1.5-fold increase at t = 1000 sec (duration = 25 sec) followed by a 3.2-fold increase in glycolysis at t = 1028 sec (duration = 45 sec). Serum [Glc] and [lactate] are 6 mM and 1 mM, respectively. Elimination of paracellular diffusion (blue dotted lines), causes predicted interstitial lactate levels to fall significantly and eliminates the lactate transient.

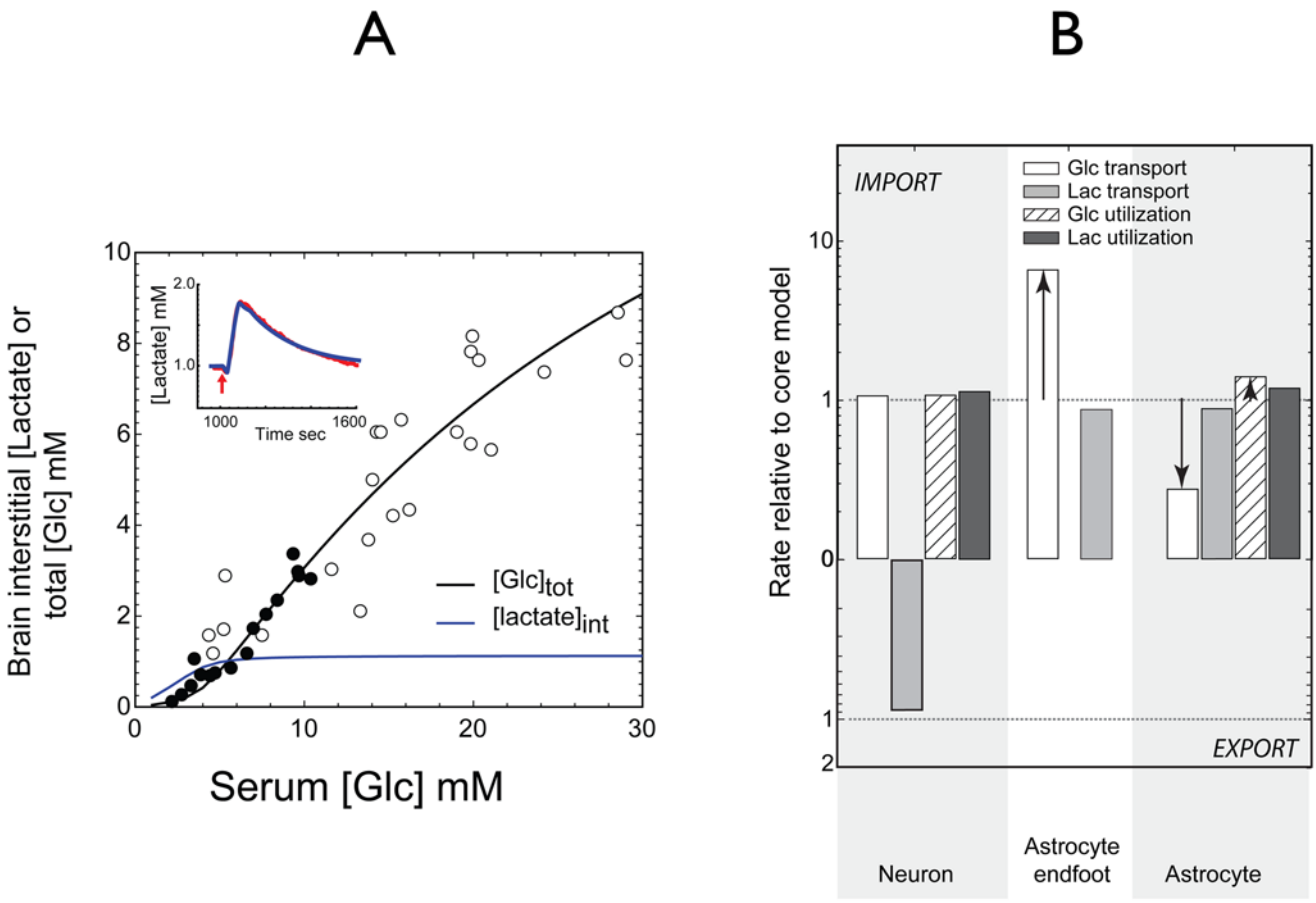

Figure 7. Simulations of brain interstitial lactate and total glucose versus serum glucose when astrocytic glucose transport capacity is increased to match neuronal glucose transport

The experiments of Figure 5 and 6 were simulated allowing for paracellular flux with two changes: 1) astrocytic glucose transport capacity was increased 12-fold to match neuronal glucose transport; 2) neuronal and astrocytic metabolic parameters were adjusted in order to reproduce the variation of brain glucose with serum glucose and lactate transients during glycolytic stimulation **A) Total brain glucose and interstitial lactate (mM) as a function of serum [Glc].** Simulations report total brain [Glc] (black lines) or interstitial [lactate] (blue lines). Data points are as described in Figure 5. The inset shows the predicted lactate transient during a 14.4-fold stimulation of astrocytic (but not neuronal) glycolysis for 45 sec preceded by a 25 sec 1.5-fold increase in neuronal and astrocytic lactate oxidation (ordinate and abscissa as in Figure 6). The red line indicates the experimental data of Hu and Wilson (see Figure 6); the blue line represents simulated interstitial lactate levels when serum [Glc] and [lactate] are 6 mM and 1 mM, respectively. **B) Adjustments in transport and metabolic flows prior to stimulation to simulate the data in panel 7A.** The ordinate indicates change in net flow of glucose and lactate at 3 membrane sites: neuron; astrocytic endfoot; astrocyte/interstitium; serum glucose 6 mM and lactate 1mM. The dashed lines indicate no change (unity). Prior to stimulation the neuron continues to export lactate and the astrocyte remains a lactate importer. Astrocytic endfoot glucose import is increased 6-fold. Astrocyte lactate import accounts for 38% of astrocytic lactate consumption. However, upon, stimulation the lactate transient is created by the astrocyte (See Figure 8B) and the lactate is taken up by the neuron thus recapitulating the postulates of the ANLS model.

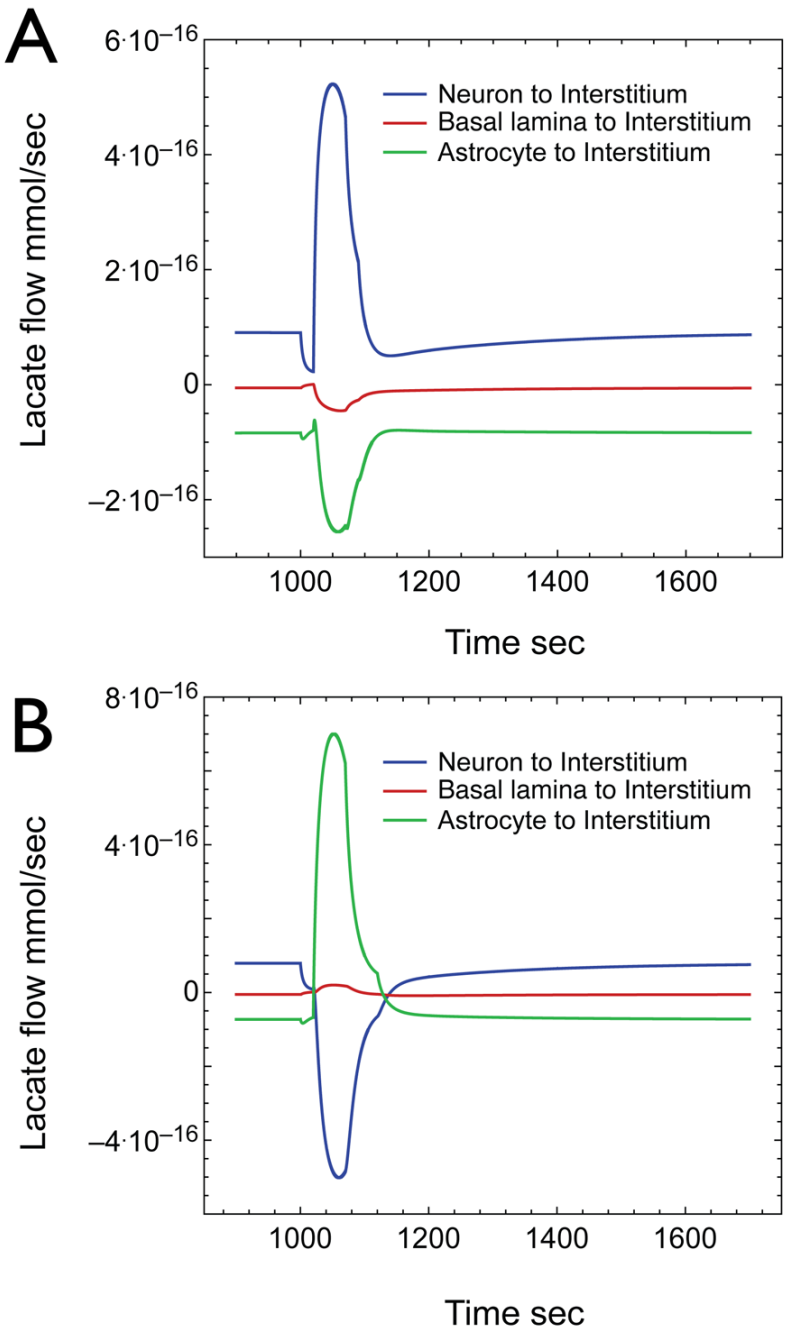

Figure 8. Contributions to interstitial lactate before and after neuronal stimulation

A) Net lactate flow in and out of the interstitium during the glycolytic step increase of Figure 6. Three lactate flows are represented: 1) net flow from astrocytes to interstitium (green line); 2) net flow from the basal lamina to interstitium (red line); 3) net flow from neurons to interstitium (blue line). Positive values indicate the direction of net flow is into the interstitium. Negative values indicate the direction of net flow is out of the interstitium. The neuron releases lactate both at rest and during stimulation while the astrocyte imports lactate both at rest and during stimulation. B) Net lactate flow into the interstitium when astrocytic glucose transport rates are increased 12-fold (see Fig 7). The neuron exports lactate before stimulation but

imports lactate during stimulation of astrocytic lactate production. The astrocyte imports lactate at rest but releases lactate during stimulation thus fulfilling the predictions of ALNS.

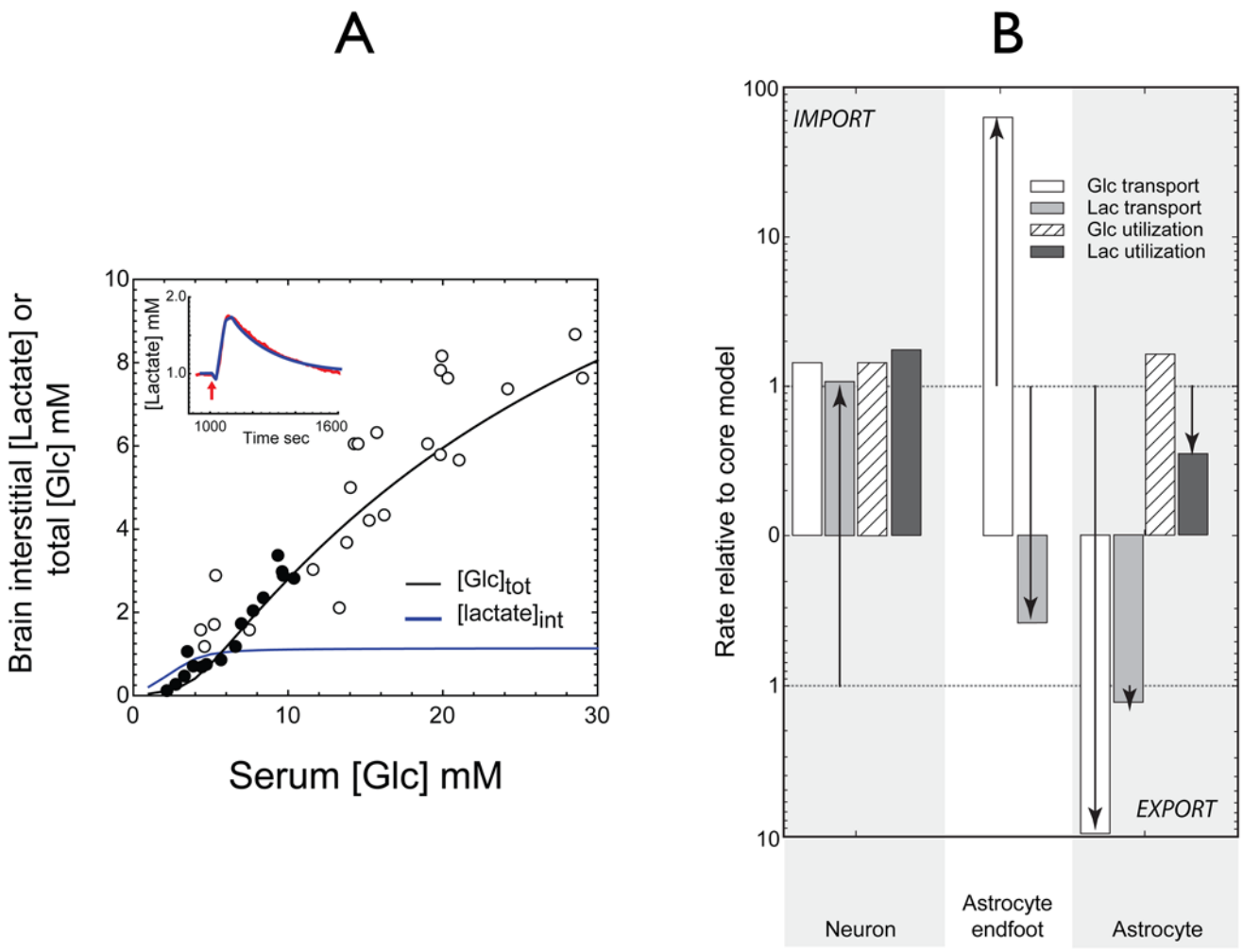

Figure 9. Simulations of total brain glucose versus serum glucose: adjustments required when diffusion is eliminated

The experiments illustrated in Figures 5 and 6 were simulated with two changes: 1) diffusion is eliminated (path 2 of Figure 3C; flows 4 and 14 of Figure 4); 2) astrocytic glucose transport, and neuronal and astrocytic metabolic parameters were adjusted in order to reproduce experimental behavior. A) Total brain [Glc] (black lines) or interstitial [lactate] (blue lines) as a function of serum [Glc]. The data points are as described in Figure 5. The inset shows the predicted lactate transient during an 8.5-fold stimulation of astrocytic (but not neuronal) glycolysis for 45 sec preceded by a 25 sec 1.5-fold increase in neuronal lactate oxidation (ordinate and abscissa as in Figure 6). The blue line represents simulated interstitial lactate levels. The red line indicates the experimental data of Hu and Wilson (see Figure 6). B) Contributions to steady-state, basal brain total [Glc] and interstitial [lactate] levels at 6 mM serum glucose and 1 mM serum lactate with adjustments in transport and metabolic flows prior to stimulation to simulate the data in panel 9A. The ordinate indicates net change in flow of glucose and lactate at 3membrane sites: neuron; astrocytic endfoot; astrocyte/interstitium. The dashed lines indicate no change (unity). The simulation required that astrocytic glucose transport capacity be increased 100-fold, astrocytic glycolytic capacity be increased by 75%, and astrocytic oxidative capacity be reduced by 66%. The neuron now imports lactate while the astrocyte exports lactate. Neuronal glycolytic and oxidative capacities were increased by

31 and 71% respectively. The astrocyte now exports glucose into the interstitium where it is imported and metabolized by the neuron to lactate.

Table 1

Glucose & Lactate Transport Capacities of Brain Cells

Cell[a]	TRANSPORTER SPECIES	[Transporter]	[Transporter]	[Transporter]	$^{b}V_{max}$ uptake	$^{b}K_m$ uptake	substrate/ ligand[c]	$^{d}k_{cat}$	^{e}predicted V_{max} in model
		pmol/ mg membrane protein	carriers/μm^2	pmol/ mg total protein	nmol/ 10^6 cells/ min	mM		per sec	mmol/sec
RBC	GLUT1	2000	2083	92	80.4	8	Glc/CB	1166	
Endothelium	GLUT1	400	1000[f]	*g 18*	*0.21*	*8*	CB	1166	7.8×10^{-15}
Astrocyte	GLUT1	7.3	18[f]	*g 0.34*	*4.8*	*8*	CB	1166	[j] 1.4×10^{-16} [k] 1.9×10^{-15}
Neuron	GLUT3	9.5	24[f]	*g 0.44*	[h] 5.0 [i] 34.6	2.8	3MG/CB	[h] 868 [i] 6512	2.3×10^{-14}
Extrapolated [MCT] values									
RBC	MCT1	3.18	8[f]	*g 0.21*	*0.133*	*4*	lactate	1166	
Endothelium	MCT1	15.5	39[f]	*g 0.71*	*10*	*4*	lactate	1166	3.0×10^{-16}
Astrocyte	MCT1/4	60.6	151[f]	*g 2.79*	*39*	*8*	lactate	1166	[j] 1.2×10^{-15} [k] 1.5×10^{-14}
Neuron	MCT2	11.7	29[f]	*g 0.54*	7.5	0.7	lactate	1166	4.9×10^{-15}

[a] Cell in which transport is measured.

[b] Measured or computed maximum rate (V_{max}) or affinity (K_m) for transport.

[c] The substrate employed in transport (Glucose (Glc), 3-O-methylglucose (3MG) or lactate) or ligand GLUT quantitation experiments (Cytochalasin B (CB) binding).

[d] Computed k_{cat} ([V_{max}/[GLUT]) for transport.

[e] Predicted V_{max} for transport of glucose and lactate for use in the model.

[f] Assumes 1 mg membrane protein is equivalent to a surface area of 2.4×10^{11} μm^2.

[g] Assumes that the ratio of membrane:total cellular protein is 0.0462 : 1.

[h] Measured at 25°C.

[i] Computed for transport at 37°C assuming that GLUT3 and GLUT1 share the same temperature dependence.

[j] Direction basal lamina to astrocyte.

[k] Direction interstitium to astrocyte. Glucose transport parameters in endothelial cells, astrocytes and neurons were computed using estimated cell membrane GLUT contents and measured k_{cat} parameters. MCT concentrations are *estimated* assuming MCT k_{cat} = GLUT1 k_{cat} and using measured V_{max} values.

Table 2

Compartment glucose levels in mM

	Primary Model[a]		ANLS[b]	
Serum [Glc]	6	30	6	30
Endothelial [Glc]	3.8	17.4	3.7	17.0
Basal lamina [Glc]	2.1	10.8	2.0	10.4
Astrocytic [Glc]	0.9	7.9	1.3	9.4
Interstitial [Glc]	1.4	9.9	1.3	9.5
Neuronal [Glc]	1.2	8.8	1.1	8.4
Brain [Glc][c]	1.2	8.9	1.2	9.1

Simulated compartment [Glc] levels (mM) predicted for

[a] the primary model of Figure 5 or

[b] the model of Figure 7 in which astrocytic GLUT1 content is increased 12-fold.

[c] Brain [Glc] represents the total [Glc] of the brain.